AE-212

Central Reactivity Measurements on Assemblies 1 and 3 of the Fast Reactor FR0

S-O. Londen

AKTIEBOLAGET ATOMENERGI

CENTRAL REACTIVITY MEASUREMENTS ON ASSEMBLIES 1 AND 3 OF THE FAST REACTOR FR0

S-O. Londen

Abstract

The reactivity effects of small samples of various materials have been measured by the period method at the core centre of Assemblies 1 and 3 of the fast zero power reactor FR0. For some materials the reactivity change as a function of sample size has also been determined experimentally. The core of Assembly 1 consisted only of uranium enriched to 20 % whereas the core of Assembly 3 was diluted with 30 % graphite.

The results have been compared with calculated values obtained with a second-order transport-theoretical perturbation model and using differently shielded cross sections depending upon sample size. Qualitative agreement has generally been found, although discrepancies still exist. The spectrum perturbation caused by the experimental arrangement has been analyzed and found to be rather important.

Introduction

The present report is based upon part of the research program in experimental reactor physics performed with the fast zero power reactor FR0 at Studsvik. A description of the reactor and reviews of the experimental work have been given in [4] and [9].

The central reactivity measurements performed on the FR0 reactor essentially consist in determining the reactivity change versus void caused by inserting a small sample of a certain material into the core centre. For some materials the reactivity change as a function of sample size has also been determined. No measurements of the reactivity change as a function of position in the reactor have been performed.

Central reactivity measurements constitute a relatively simple and accurate form of integral experiments. With these measurements it is possible to check the group cross sections, the calculated spectra, and to some extent the perturbation methods used in the analysis. The measurements reported here were carried out in two series, the first on an undiluted core consisting only of uranium with an enrichment of 20 % (Assembly 1), the second on a core diluted with 30 % graphite (Assembly 3). The compositions and critical dimensions of the systems are given in Appendix 1.

1. Perturbation theory and methods of analysis

1.1 General theory

Before examining the different methods of analysis used to obtain calculated central reactivity coefficients it is important to note that the perturbation concept will be used for three different phenomena.

Starting from a homogeneous system the experimental arrangement causes the first perturbation and the term reference system used below in this section denotes a system already perturbed in this way.

The sample inserted into the core centre causes an additional flux perturbation, and this flux perturbation, $\Phi^P - \Phi$, appears in the expressions below for the change in eigenvalue. It is however, convenient to separate this perturbation into two parts. The fine-structure perturbation caused by the resonance structure of the cross sections of the sample

will be taken into account by using appropriately shielded cross sections, and the theory developed in this section is used for the third perturbation, i.e. for calculating the perturbations of the group fluxes.

As usually, we assume that the neutron flux can be represented by the ordinary linear Boltzmann transport equation and consider a source--free stable reference system and a perturbed system with the multiplication factor $k = k^P$. The perturbed flux is assumed to be transient--free with an exponential time-dependence. By proceeding as in [8] we obtain a perturbation expression for Δk:

$$N\Delta k = \iiint \Phi^+(\bar{r}, E)\Delta[\nu(E')\Sigma_f(E')\chi(E'E)+\Sigma(E'E)]\Phi^P(\bar{r}, E')drdE'dE$$

$$- \iiint \Phi^+(\bar{r}, E, \Omega)\Delta\Sigma_t(E)\Phi^P(\bar{r}, E, \Omega)d\bar{r}dEd\Omega \qquad (1)$$

which is related to the reciprocal period α by effective delayed neutron fractions β and by an effective prompt neutron generation time ℓ. The values have been computed for FR0 and are reported in [12]. Strictly speaking β and ℓ depend on all flux perturbations but this dependence will here be ignored. We also assumed that the same β-values can be used in Assemblies 1 and 3.

In (1) N is the normalization integral,

$$N \equiv \iiiiint \Phi^+(\bar{r}, E, \Omega)\nu(\bar{r},E')\Sigma_f(\bar{r}, E')\chi(\bar{r}, E', \Omega', E, \Omega)\Phi^P(\bar{r}, E', \Omega')d\bar{r}dE'd\Omega'dEd\Omega$$

Φ^+ is the adjoint flux of the reference system and Φ^P is the regular perturbed flux. The cross sections follow the usual notation, Σ_t is the total cross section, Σ the scattering cross section and Σ_f the fission cross section. ν is the average number of neutrons per fission and χ the fission spectrum.

If Φ^P in (1) is replaced by Φ, the unperturbed regular flux, as is usually done, we get the first order perturbation equation. This corresponds to performing the reactivity measurements on an infinitesimally small sample which does not perturb the reference flux. Of course this is not possible - to get acceptable accuracy the samples used in fast spectra must be rather large. Replacing Φ^P by Φ thus implies neglecting all sample size effects and may lead to serious errors in the analysis.

On the other hand analysis by means of perturbation techniques rapidly loses its justification if the flux is perturbed too much, i.e. if Φ^P cannot be computed from Φ. An optimum sample volume should thus be chosen keeping in mind the two requirements; good experimental accuracy and acceptable flux perturbation caused by the sample.

1.2 Second order perturbation models

Hansen and Maier [8] have proposed a second-order perturbation model for calculating Φ^P for small material replacements and this model has been developed in two codes for spherical and cylindrical samples, respectively. No attempt has been made to analyze exactly the validity limits of the mathematical model.

The first code, PERCYL, is intended for use with 6-group two-dimensional S_N fluxes and cylindrical samples. The code needs the following fluxes

$$\Phi(r, z, E, \Omega) \qquad \Phi^+(r, z, E, \Omega)$$

$$\Phi(r, z, E) \qquad \Phi^+(r, z, E)$$

which should be defined at a number of points in a four-dimensional (r, z, E, Ω) lattice. The output includes the reactivity and the perturbed angular and total regular fluxes, $\Phi^P(r, z, E, \Omega)$ and $\Phi^P(r, z, E)$. This second-order transport-theoretical code has been used with the 6-group S_N fluxes (items 1 and 2 in the list of fluxes available, Section 1.4) and the 6-group cross sections, obtained from the Häggblom set (see Section 1.3), to calculate reactivity equivalences for the samples tested.

A simpler second-order perturbation code for spherical samples, PERS, has also been written using basically the same approach. This code was used with the 17-group MUCC-fluxes (item 4 in the list of fluxes available, Section 1.4) and the Bondarenko cross sections (see Section 1.3) to calculated reactivity equivalences for the samples. The cylindrical samples were then approximated to spheres by equating the average chord lengths $\bar{\ell} = 4V/A$.

The normalization integrals N were computed with the various S_N fluxes using two codes (spherical and cylindrical geometry) written for the IBM-7044 machine [2].

A detailed description of the second-order perturbation codes is given in [2].

1.3 Cross sections

The group cross sections now in use for all flux calculations on the FR0 reactor are based upon differential data compiled by Häggblom. The sources from which the data are taken are given in [12]. The data are used in the NESPECO code [11], written for the Ferranti-Mercury computer, to calculate group cross sections. In this code the differential data are weighted with a fine-structure flux calculated for the core composition in question. The differential cross sections are not weighted by a product of the regular and adjoint fluxes, which may be of some importance in the perturbation calculations. The number of groups usually chosen is 14 and 6. Anisotropic scattering is taken into account by the transport cross section for scattering within a group, but scattering to other groups is assumed to be isotropic. The differential data used are not shielded except for the U238 data [12]. The group sections of any other element obtained with the code are shielded to the extent that the resonances of the element in question coincide with dips in the fine-structure flux. It is essential to note that all the flux calculations mentioned in this report have been performed with this same cross section set, although the number of groups may vary.

To obtain calculated reactivity coefficients the Häggblom set and the new Bondarenko 26-group cross section set [6] were used. The groups 1-17 of the Bondarenko set, i.e. down to 100 eV, were introduced here. As these group cross sections, except for the three highest groups, are simply lethargy averages, the same set must be used in both assemblies. Of course the Häggblom set should give more reliable group cross sections as the differential data are weighted with an accurate fine-structure flux.

The two principal reasons for using the Bondarenko set were:

a)   The Häggblom set does not contain all the materials tested in these measurements, whereas the Bondarenko set does.

b)   The Bondarenko set offers a convenient possibility of taking the resonance structure of the cross sections of all the materials into account.

The resonance structure is taken into account by the $f(\sigma_o)$ co-efficients, or self-shielding coefficients for a certain element. The definition of σ_o which applies to a homogeneous medium is modif'ed for the small samples used here. As suggested in [6] σ_o is replaced by σ_o^{*}, defined as

$$\sigma_o^{*} = \sigma_o + \frac{1}{\rho\bar{\ell}} \qquad (2)$$

where

ρ = density of nuclei of the particular element in the sample,

$\bar{\ell}$ = average chord length of sample = $4V/A$,

σ_o = sum of the total cross sections of all the other elements in the sample referred to a single atom of the element in question.

From (2) $f(\sigma_o^{*})$ and shielded cross sections for all the materials tested have been computed. Slightly different cross sections are thus obtained for the same material, depending upon sample size. The use of the f-coefficients is to some extent arbitrary as they are given only for certain σ_o-values; the interpolation necessary may lead to some errors.

The energy limits of the 6 and 14 groups mentioned above are given in Appendix 2.

1.4 Flux calculations

The different numerical multigroup methods ordinarily in use at the FR0 reactor for criticality and flux calculations have been listed in [4]. The two-dimensional TDC code has now been slightly modified so that the regular and adjoint angular fluxes may also be obtained.

For the analysis of the central reactivity measurements the following flux calculations were available:

1. 6-group TDC calculations on an unperturbed (no experimental arrangement) cylindrical assembly.

2. 6-group TDC calculations on an assembly containing the experimental arrangement B. Fig. 7 gives the geometry of the arrangement.

3.   14-group DSN calculations on an unperturbed spherical assembly.

4.   17-group MUCC calculations on an unperturbed spherical assembly.

For each of the four types of flux calculations listed above regular and adjoint fluxes with the compositions of Assemblies 1 and 3 were available. The calculated central regular and adjoint spectra for Assemblies 1 and 3 are given in Figs. 1 and 2. The calculated regular group fluxes along the central vertical axis in an Assembly with channel B are given in Figs. 3 and 4 for Assemblies 1 and 3, respectively.

2.   Experimental

2.1 _Experimental arrangement

The reproducibility of the positions of the reactor halves and the control rods after shut-down does not permit a more accurate reactivity determination than 1-2 pcm $(1 \text{ pcm} = 10^{-5})$ without remote control. As the reactivities measured were often < 5 pcm, it is obvious that the reactor could not be shut down between the measurements which implies that the reactivity changes must be made by remote control.

An automatic 4-chamber sample changer, manoeuvred from the control room, was therefore used (Fig. 5). One chamber was used as a reference chamber while the three others contained various samples. The whole changer can be moved in a vertical direction and, using microswitches and relay automatics, the cross can be turned in steps of 90°. The fixed Al bars of the cross are approximately 30 cm in length and different tubes or bars can be attached to them. The samples, placed in the small chambers, were moved into and out of the core centre through central vertical experimental channels and the measurements of the reactivity differences between the chambers containing the samples and the empty reference chamber could thus be performed without shutting down the reactor between the measurements.

Two experimental channels were used, here denoted A and B. Channel A, with section area 2.86 x 2.86 cm^2 in the core, was used for most of the measurements, whereas channel B, with section area 4.6 x 4.6 cm^2, was used for some materials when determining the reactivity change as a function of sample size.

The main features of channel A are shown in Fig. 6 (Figs. 6 and 7 both show the channels in Assembly 1. Exactly the same experimental arrangements were used in Assembly 3). Through the Cu plates constituting the reflector above the core a cylindrical hole has been drilled and the channel in the core can be built up of fuel plates on the module system. Fig. 6 also shows the Al tube which is attached to the fixed part of the sample changer and the solid brass bar which is used to prevent neutron streaming through the hole. The brass chamber in which the samples are contained is screwed to the solid brass bar. Fig. 8 a shows a full-scale horizontal section at the centre plane of the central fuel element with channel A. The inside diameter of the sample chamber is 22 mm, the chamber height twice the module height or 86 mm, and the brass wall is 1.5 mm thick. An Al tube and four thin Cu tubes fix the fuel plates. Most of the central reactivity measurements performed with channel A were done with samples which filled the whole chamber, but for some materials with large reactivity equivalences per gram smaller samples were used. The reactivity measurements as a function of sample size made with channel A were done by varying the diameter of the cylindrical samples.

The main features of channel B are shown in Fig. 7. To make measurements of larger samples possible, the whole central fuel element has now been removed. Four steel tubes are attached to the fixed part of the sample changer and to these steel tubes truncated fuel elements are screwed. The truncated fuel elements contain the Cu plates which prevent neutron streaming and below the Cu plates is the sample chamber. The height of a sample chamber is again twice the module height or 86 mm. The Cu plates and the sample to be measured are fixed in position by thin steel rings of height equal to one sixth the module height, i.e. 7 mm, which are piled vertically in the chamber. The steel frames of the truncated fuel element are held together by the steel construction below the chamber. Finally, below the whole channel is placed another truncated fuel element containing the appropriate loading of fuel and reflector material.

The samples measured in channel B were usually available in the same size as ordinary fuel plates, i.e. with dimensions 4.3 x 4.3 x x 0.7 cm^3. The plates were then piled horizontally in the chamber, re-

placing the thin steel rings. The reactivity measurements as a function of sample size performed in channel B were thus made by varying the height of the samples. By combining the steel rings and thin circular Cu plates, small cylindrical containers for powdered material could be obtained.

Fig. 8 b shows a full-scale horizontal section of an empty sample chamber in channel B at the centre plane.

For safety reasons the automatic sample changer was not used for measuring the reactivity equivalence of a Pu sample. Of course, by shutting down the reactor the measurements lose somewhat in accuracy, but on the other hand the flux perturbation caused by the experimental arrangement is much smaller when the sample changer is not used. The experimental error was now only 1 %, as the sample has a reactivity equivalence of the order of 100 pcm.

A complete list and description of the samples tested is given in Tables 1-3.

Table 1   Samples measured in channel A

Label of sample and isotopic composition	Shape *)	R [mm]	H [mm]	Total weight g
U238-1 0.491% U235	P	-	43	82
U235-1 20% U235	P	-	43	81
Th232-1	C	11	86	354
W-1	C	11	86	191
Ta	C	11	35	215
Mo	C	11	86	237
Nb_2O_5	C	11	86	58
Zr	C	11	86	82
Cu-1	C	10.9	86	281
Cu-2	C	10.0	86	239
Cu-3	C	8.5	86	172
Cu-4	C	6.5	86	102
Cu-5	C	5.0	86	60
Cu-6	C	3.0	86	22
Ni	C	11	86	109
Fe-1	C	11	86	247
Cr	C	11	86	108
V	C	11	86	107
Ti	C	11	86	77
Al-1	C	11	86	85
CuO	C	11	86	26
C-1	C	11	86	42
B-1 (nat. boron)	C	10.8	48	6.5
B-2 -"-	C	8.2	50	4.6
B-3 -"-	C	5.1	52	2.1
B-10 (91 % B10)	C	5.1	52	2.9
D_2O	C	5.1	52	5.0
Diphenyl-1 $(C_6H_5-C_6H_5)$	C	10.8	48	9.5
Diphenyl-2 $(C_6H_5-C_6H_5)$	C	8.2	50	7.2
Diphenyl-3 $(C_6H_5-C_6H_5)$	C	5.1	52	2.8

Table 2   Samples measured in channel B

Label of sample and isotopic composition	Shape[x]	R [mm]	H [mm]	Total weight, g
U238-2 Natural U	P		43	1481
U238-3 " "	P		22	743
U238-4 " "	P		7	248
Th232-2	4C[xx]			711
Th232-3	2C[xx]			354
Th232-4	C[xx]			177
W-2	C	21	43	272
W-3	C	21	22	123
W-4	C	21	7	31
Fe-2	P		43	604
Fe-3	P		22	302
Fe-4	P		14	201
Fe-5	P		7	101
Al-2	P		86	423
Al-3	P		43	212
Al-4	P		22	106
Al-5	P		14	71
Al-6	P		7	35
C-2	P		43	132
C-3	P		22	66
C-4	P		14	45
C-5	P		7	23

Table 3   Sample measured by shutting down the reactor between the measurements

Label of sample and isotopic composition	Shape[x]	R [mm]	Total weight, g

Pu
    95 % Pu239
    4.7 % Pu240
    0.3 % Pu241
	S	10	62

[x] S = Spherical
   P = Parallelepipedic
   C = Cylindrical

[xx] The Th-2, Th-3 and Th-4 samples consisted of four, two and one cylinders (H = 43 mm, R = 11 mm), respectively, which were placed horizontally in the chamber.

The horizontal section of the parallelepipedic plates was
43×43 mm^2, except for the U238-1 and U235-1 samples which had a
section of 7×14 mm^2. As the samples measured in Assemblies 1 and
3 were not always exactly identical in weight, the values given in Tables
1-3 are average weights.

2.2 _ Experimental method

The reactivity measurements were made by the positive period
method. Two runs per sample were usually made, whereas the reference
chamber was measured three of four times at suitable intervals to check
the stability of the system.

A serious problem encountered during the measurements was the
dependence of the reactivity on temperature. The experiments showed
that the reactivity of the assembly as a whole increases continuously
during the first 8-10 hours of operation. This is due to the heat genera-
tion in the magnets which keep the safety rods in their "in" positions.
The total amount of the reactivity increase is about 2-3 pcm. One would
expect the opposite sign for this effect as the temperature coefficient of
the system is negative [9]. The reactivity increase depends, however,
upon the thermal expansion which forces the reactor halves closer to-
gether. As the experimentally determined value of the reactivity equiv-
alence of the air gap is 200 pcm/mm [9] a displacement of only 10^{-2} mm
is required. To avoid such an instability, the safety rods were kept in
their "in" positions day and night during the measurements. The temper-
ature stability of the reactor is good when the ten hours have elapsed, as
the temperature in the reactor hall is well regulated.

For the doubling time measurements a U235 fission counter placed
in the reflector was used as detector. The detector was coupled to a
RAMSES data collecting and recording equipment [5], which in this mode
alternatively counted for a preset time in one channel while registering
the content in another, and vice versa. The reactivity was calculated
from the data by a code, REMI-FR0, written for the Ferranti-Mercury
computer [1]. Of course the fundamental assumption that the flux rises
exponentially is not satisfied shortly after the reactivity increase, and
due to spontaneous fission the reactor is slightly subcritical by approx-
imately 0.8 pcm when the power is stabilized at 0.01 W. These error

sources have been taken into consideration by omitting the starting data according to [13].

The reproducibility of the reactivity measurements has proved to be approximately $\pm$ 0.05 pcm. The error is partly a statistical error and partly due to temperature effects. Compared to these error sources the irreproducibility of the position of the Cu bar is negligible. The total errors of the results given below in chapter 4 have been obtained by dividing 0.08 pcm by the respective sample weights.

3.   Numerical procedures used for calculating reactivity coefficients

It has been the aim throughout this work to compare the actual experimental values, uncorrected for sample size effects or for perturbations caused by the experimental arrangements, with calculated values which take these perturbations into account.

Two different sets of reactivity coefficients have been computed, called sets C1 and C2. Both sets are corrected for the flux perturbations caused by the experimental arrangement, for the resonance self-shielding of the samples and for the group flux perturbations caused by the samples. The deviations between the two sets can thus be assigned to differences in differential data, flux weighting within the groups, and number of groups.

Set C1 is obtained with the PERCYL code using the Häggblom cross section set, the 6-group TDC fluxes available (items 1 and 2 in 1.4) and the actual sample dimensions. (Parallelepipedic samples were approximated by cylinders.) The values thus obtained were then corrected for resonance self-shielding effects. The interpolation necessary to account for the flux depression caused by channel A, for which no flux calculations were made, was accomplished by measurements and calculations of the fuel reactivity coefficient in the different channels.

It is important to note that the interpolation was not equivalent to the assumption that all materials were affected by the experimental arrangement in the same way as U235.

A serious objection that may be raised against the interpolation procedure is that no account has been taken of the spectrum perturbation caused by the brass wall and the Al tube surrounding the sample in channel A. These perturbing factors do not appear in channel B and the

U235 coefficient measured in channel A is quite insensitive to a slight inelastic scattering in the walls. It is possible that this slight spectrum shift causes some errors.

Set C2 uses the Bondarenko group cross sections, with different self-shielding coefficients depending upon sample size, as explained in 1.3. Together with the 17-group fluxes in the core centre obtained by MUCC calculations (item 4 in 1.4) and equivalent sample radii these cross sections were used in the PERS code. The values thus obtained were then corrected for the perturbation caused by the experimental arrangement.

Some first-order perturbation calculations were made to examine the effect of reducing the number of groups from 14 to 6 in the Häggblom cross section set using the spherical and cylindrical S_N fluxes for unperturbed assemblies (items 1 and 3 in 1.4). Finally, some first-order calculations have also been made with 14-group diffusion-theoretical fluxes to trace any possible differences resulting from the use of two codes based on different principles.

4. Experimental results and calculated values

The experimental results and the calculated values as obtained by the procedure described in chapter 3 are given in Tables 4 and 5. It should be noted that all samples measured in Assembly 1 were not measured in Assembly 3, and vice versa. The samples are listed in order of decreasing atomic weight of the principal constituent. It has generally not been considered appropriate to calculate reactivity coefficients of the elements or isotopes appearing in compounds or mixtures, because of the sample size dependence encountered. Only two exceptions are given at the end of Table 4.

It is difficult to compare directly the values in pcm/g obtained for the same material in Assemblies 1 and 3 because of the different normalization integrals N. The experimental values have therefore also been converted to effective cross sections by equating the calculated reactivity equivalences of Pu239 in the different channels in Assembly 1 to + 3.35 b and in Assembly 3 to + 3.36 b. These values were obtained by weighting $(\nu-1-\alpha)\sigma_f$ with the spectrum at the core centre. The cross sections are given in Table 6 and the values in the two Assemblies are now directly comparable.

Table 4   Experimental and calculated central reactivity coefficients in channel A.
All value in pcm/g

Label of sample	Assembly 1			Assembly 3		
	Exp.	C1	C2	Exp.	C1	C2
U238-1	- 0.027 ± 0.001	- 0.029	- 0.026	- 0.033 ± 0.001	- 0.027	- 0.034
U235-1	+ 0.229 ± 0.001	+ 0.223	+ 0.233	+ 0.150 ± 0.001	+ 0.155	+ 0.164
Th232-1	- 0.125 ± 0.0002		- 0.136	- 0.101 ± 0.0002		- 0.113
W-1	- 0.110 ± 0.0004		- 0.124	- 0.087 ± 0.0004		- 0.100
Ta	- 0.231 ± 0.0004		- 0.216	- 0.200 ± 0.0004		- 0.190
Mo	- 0.120 ± 0.0003		- 0.124	- 0.093 ± 0.0003		- 0.096
Zr	+ 0.031 ± 0.001	- 0.039	- 0.056	+ 0.057 ± 0.001	- 0.019	- 0.035
Cu-1	- 0.101 ± 0.0003	- 0.099	- 0.090	- 0.066 ± 0.0003	- 0.076	- 0.060
Cu-2	- 0.101 ± 0.0003	- 0.099	- 0.092	- 0.066 ± 0.0003	- 0.078	- 0.062
Cu-3	- 0.106 ± 0.0003	- 0.101	- 0.095	- 0.067 ± 0.0005	- 0.080	- 0.064
Cu-4	- 0.110 ± 0.0008	- 0.103	- 0.097	- 0.068 ± 0.0008	- 0.082	- 0.065
Cu-5	- 0.112 ± 0.001	- 0.106	- 0.100	- 0.069 ± 0.001	- 0.084	- 0.068
Cu-6				- 0.070 ± 0.003	- 0.087	- 0.071
Ni	- 0.116 ± 0.0007	- 0.126	- 0.119	- 0.065 ± 0.0007	- 0.089	- 0.072
Fe-1	- 0.069 ± 0.0003	- 0.051	- 0.060	- 0.038 ± 0.0003	- 0.029	- 0.035
Cr	- 0.068 ± 0.0008	- 0.076	- 0.081	- 0.035 ± 0.0008	- 0.038	- 0.046
V	- 0.019 ± 0.0008		- 0.046			
Ti	- 0.066 ± 0.001		- 0.059			

contd.

Table 4   contd.

Label of sample	Assembly 1			Assembly 3		
	Exp.	C1	C2	Exp.	C1	C2
Al-1	- 0.034 ± 0.0009	- 0.031	- 0.015	- 0.025 ± 0.0009	- 0.016	- 0.025
C-1	+ 0.177 ± 0.002	+ 0.187	+ 0.218	+ 0.114 ± 0.002	+ 0.109	+ 0.110
B-1	- 2.51 ± 0.01	- 2.72	- 2.03	- 2.27 ± 0.01	- 2.67	- 2.15
B-2	- 2.52 ± 0.02	- 2.70	- 2.04	- 2.34 ± 0.02	- 2.65	- 2.16
B-3	- 2.46 ± 0.04	- 2.72	- 2.03	- 2.31 ± 0.04	- 2.68	- 2.15
B-10	-13.7 ± 0.03		- 10.9	-12.5 ± 0.03		- 11.0
D_2O	+ 1.43 ± 0.02	+ 1.22	+ 1.60	+ 0.768 ± 0.016	+ 0.638	+ 0.701
Diphenyl-1	+ 3.82 ± 0.008	+ 2.73	+ 3.58	+ 3.44 ± 0.008	+ 1.52	+ 2.35
Diphenyl-2	+ 3.64 ± 0.01	+ 2.72	+ 3.55			
Diphenyl-3	+ 3.38 ± 0.03	+ 2.73	+ 3.45	+ 3.19 ± 0.03	+ 1.53	+ 2.23
CuO	- 0.062 ± 0.003	- 0.082	- 0.048	- 0.043 ± 0.003	- 0.069	- 0.043
O	+ 0.138		+ 0.014	+ 0.184	+ 0.061		- 0.009	+ 0.102
Nb_2O_5	- 0.088 ± 0.001		- 0.070			
Nb	- 0.185		- 0.179			

Table 5 Experimental and calculated central reactivity coefficients in channel B. All values in pcm/g.

Label of sample	Assembly 1			Assembly 3		
	Exp.	C1	C2	Exp.	C1	C2
U238-2	- 0.026 ± 0.0001	- 0.028	- 0.027			
U238-3	- 0.023 ± 0.0001	- 0.024	- 0.025			
U238-4	- 0.016 ± 0.0003	- 0.021	- 0.022			
Th232-2	- 0.106 ± 0.0001		- 0.123			
Th232-3	- 0.110 ± 0.0002		- 0.124			
Th232-4	- 0.116 ± 0.0004		- 0.129			
W-2				- 0.082 ± 0.0003		- 0.093
W-3				- 0.081 ± 0.0007		- 0.094
W-4				- 0.081 ± 0.003		- 0.095
Fe-2	- 0.063 ± 0.0001	- 0.045	- 0.050	- 0.035 ± 0.0001	- 0.027	- 0.031
Fe-3	- 0.065 ± 0.0003	- 0.049	- 0.053	- 0.038 ± 0.0003	- 0.030	- 0.033
Fe-4	- 0.068 ± 0.0004	- 0.051	- 0.054			
Fe-5	- 0.073 ± 0.0008	- 0.054	- 0.058	- 0.039 ± 0.0008	- 0.032	- 0.035
Al-2	- 0.027 ± 0.0002	- 0.022	- 0.030			
Al-3	- 0.021 ± 0.0004	- 0.026	- 0.031			
Al-4	- 0.009 ± 0.0008	- 0.028	- 0.030			
Al-5	+ 0.003 ± 0.001	- 0.027	- 0.030			
Al-6	+ 0.033 ± 0.002	- 0.027	- 0.029			
C-2	+ 0.148 ± 0.0006	+ 0.191	+ 0.226	+ 0.101 ± 0.0006	+ 0.090	+ 0.103
C-3	+ 0.170 ± 0.001	+ 0.185	+ 0.223	+ 0.098 ± 0.001	+ 0.089	+ 0.100
C-4	+ 0.181 ± 0.002	+ 0.183	+ 0.221			
C-5	+ 0.229 ± 0.003	+ 0.181	+ 0.219	+ 0.095 ± 0.003	+ 0.089	+ 0.099

Table 6   Experimental effective cross sections.
           All values in mb

Label of sample	Assembly 1	Assembly 3
U238-1	- 41	- 74
U238-2	- 43	
U238-3	- 38	
U238-4	- 26	
U235-1	+ 352	+ 335
Th232-1	- 187	- 221
Th232-2	- 170	
Th232-3	- 176	
Th232-4	- 186	
W-1	- 131	- 150
W-2		- 149
W-3		- 147
W-4		- 147
Ta	- 271	- 340
Mo	- 75	- 84
Zr	+ 18	+ 48
Cu-1	- 41	- 39
Cu-2	- 41	- 39
Cu-3	- 43	- 40
Cu-4	- 45	- 40
Cu-5	- 46	- 41
Cu-6		- 41
Ni	- 44	- 36
Fe-1	- 25	- 20
Fe-2	- 24	- 19
Fe-3	- 25	- 21
Fe-4	- 26	
Fe-5	- 28	- 21
Cr	- 22	- 17
V	- 6	
Ti	- 20	
Al-1	- 6	- 6
Al-2	- 5	
Al-3	- 4	
Al-4	- 2	
Al-5	+ 1	
Al-6	+ 6	
C-1	+ 14	+ 13
C-2	+ 12	+ 12
C-3	+ 14	+ 12
C-4	+ 15	
C-5	+ 19	+ 11

Contd.

Table 6   contd.

Label of sample	Assembly 1	Assembly 3
B-1	- 175	- 231
B-2	- 176	- 238
B-3	- 172	- 235
B-10	- 896	-1189
D_2O	+ 185	+ 144
Diphenyl-1	+ 381	+ 498
Diphenyl-2	+ 364	
Diphenyl-3	+ 337	+ 462
CuO	- 32	- 32
O	+ 14	+ 9
Nb_2O_5	- 151	
Nb_2O_5	- 111	

5.   Discussion of results

5.1 _ U235 and U238

U235

As can be seen in Table 4 the agreement between the experimental and the computed values is rather good for U235 and, by using a higher number of groups in set 2, still better agreement is attained in both assemblies. The Bondarenko group cross sections - with the exception of the three highest groups - are lethargy averages and not weighted with a correct flux. It is thus to be expected that this set gives reactivity coefficients which are slightly too high as σ_f rises from 1.2 b at 1 MeV to approximately 2.5 b at 20 keV while the real flux, as can be seen in Fig. 1, decreases rapidly. The median energy of the neutrons causing fission in U235 in the core centre is about 360 keV in Assembly 1 and 240 keV in Assembly 3.

U238

The reactivity effects caused by inserting U238 samples in fast reactor spectra are relatively complex. The central reactivity coefficient should be viewed as the sum of a large positive term caused by fission, of a large negative term caused by capture, and of a term caused by down-scattering, which may be either positive or negative as the reactivity contribution due to scattering is determined by the difference between the values of the adjoint spectrum at the final and initial energies and directions of the neutron. Small errors in the cross sections and fluxes used are therefore greatly enlarged in the calculation of the reactivity coefficient.

The small discrepancies between experimental and computed values for depleted uranium (Table 4) should be analyzed keeping this in mind and it seems that the agreement is satisfactory. The low C1 coefficient in Assembly 3 seems again to be rather dependent on the number of groups used in set 2. A comparison between the two experimental values shows the effect of the reduced positive reactivity contribution due to fission and the increased negative contribution due to capture in Assembly 3.

Some measurements of the reactivity equivalence of natural uranium as a function of sample size were made in Assembly 1 (Table 5 and

Fig. 9a). The increasing negative reactivity coefficient is explained by the decreasing contribution of fission, as the inelastic scattering rapidly reduces the flux above the fission threshold. The sample size dependence has not been quite satisfactorily reproduced by calculations - the dependence seems to be more pronounced for natural uranium than the used model predicts.

5.2 Strong, heavy absorbers

Th

Although thorium is fissionable at high energies, the predominant reactivity effect is capture. σ_c rises from 0.1 b at 1 MeV to 1 b at 10 keV and the reactivity coefficient measures the low-energy part of the spectrum. At higher energies the reactivity contributions due to inelastic scattering and fission tend to cancel in the spectra examined here.

A comparison of the experimental effective cross sections for the sample Th232-1 in Assemblies 1 and 3 (Table 6) shows the spectrum shift towards lower energies.

The small absolute discrepancies between calculated and experimental values (Table 4) may partly be explained by uncertainties in the differential cross sections, partly by the absence of correct flux weighting in the Bondarenko set, and the low-energy flux - or, more exactly, $\Phi\Phi^+$ in this range - seems to be correctly calculated.

Some measurements of the reactivity coefficient of Th as a function of sample size have been performed in Assembly 1 (Table 5 and Fig. 9b). The decreasing reactivity coefficient with increase of sample size supports the assumptions that fission is always of secondary importance compared to absorption and that the down-scattering cannot compensate the absorption in the lower energy groups. The calculations seem to reproduce the sample size dependence for Th-samples satisfactorily.

W

σ_c of tungsten rises from 0.1 b at 1 MeV to 0.7 b at 10 keV and W is thus also more sensitive to the low-energy part of the spectrum.

In addition, inelastic scattering has a cross section of 2.5 b above 1 MeV. A comparison of the calculated and experimental values in Table 4 reveals that the Bondarenko set again slightly overestimates the absorption, partly because of the absence of correct flux weighting. However, the discrepancy is of the same magnitude as the uncertainties concerning the cross sections.

The measurements made with different sample sizes in Assembly 3 (Table 5) show that the reactivity coefficient is almost independent of sample size.

Ta

Tantalum has a considerably larger absorption cross section than Th and W. σ_c is about 0.14 b at 1 MeV and 2 b at 10 keV. A comparison between the experimental and calculated values given in Table 4 shows in this case a systematic discrepancy of about 5 %. The discrepancy is of opposite sign to that of Th and W. It is interesting to note that this result is consistent with the values obtained at the ZPR-III assemblies [7]. In the latter the ratio between the experimental and calculated values has on the average been 10-20 % higher for Ta than for other heavy absorbers (Th, Mo and Nb). The possibility that the capture cross sections of Ta given in Bondarenko are somewhat too low, at least compared to the Th and W cross sections, cannot be excluded.

Mo

Molybdenum shows similar properties to tungsten. The capture cross section is 0.03 b at 1 MeV and 0.3 b at 10 keV. The measured spectrum degradation is well reproduced by the calculations and the small absolute discrepancies are again of the same magnitude as the uncertainties concerning the cross sections.

Nb

Niobium has a capture cross section of about 0.03 b at 1 MeV and about 0.8 b at 10 keV. An attempt to measure the reactivity coefficient of Nb in Assembly 1 was made with Nb_2O_5, but because of the expected strong dependence of the oxygen coefficient on sample size the results

should be carefully analyzed. No measurements with Nb have been per-formed in Assembly 3.

The results are shown in Table 4. The oxygen coefficients obtained with the Cu-5 and CuO samples have been used for the Nb values. The slight discrepancy is of opposite sign compared with the results obtained with other heavy absorbers, but it is probable that the reactivity coef-ficient of oxygen is smaller in Nb_2O_5 than in CuO. If the oxygen coeffi-cient used, +0.138 pcm/g, is reduced by 20 %, the experimental Nb coef-ficient is reduced to - 0.173 pcm/g instead of - 0.185 pcm/g. This would give the small discrepancy the same sign.

The Nb result also shows that $\Phi\Phi^+$ in the low-energy part of the spectrum in the core centre is well predicted by calculations.

5.3 _Intermediate absorbers_

Cu

Copper measurements have a particular interest for the FR0 work because of the large discrepancies between experiments and calculations found in the low-energy part of the copper reflector spectrum [4], [3].

It was therefore considered worth while to perform a series of measurements with Cu samples of different size to examine whether any discrepancies could be found also in the central reactivity measure-ments.

The capture cross section of Cu is about 0.005 b at 2.5 MeV and then rises to 0.1 b at 10 keV. The magnitude of the measured effective cross sections (Table 6) shows that a large part is now caused by in-elastic scattering, the effective capture cross section alone being about 18 mb.

As will be seen from Table 4 and Fig. 10a, the agreement between the experimental and calculated values in Assembly 1 is acceptable al-though small discrepancies exist. The difference between the calculated values is due to the large σ_c of the Häggblom set above 500 keV and in the range 30-70 keV. Reducing the C1 value slightly leaves absolute discrepancies of about 10 %. It is possible that the inelastic cross sec-tions in both sets used are somewhat underestimated. This would be consistent with the results reported in [10]. The rather strong sample size dependence measured, slightly more pronounced than calculations

indicate, does not contradict this assumption as more than half of the calculated sample size dependence in Assembly 1 is caused by perturbation of the group fluxes, mainly by reduction of the high-energy flux.

But the discrepancies are larger in Assembly 3. An examination of the results obtained with the samples Cu-5 and Cu-6, for which the corrections needed for the finite sample size are small, reveals that the C1 value gives a too negative reactivity coefficient. It should be noted that the small discrepancy between the C1 value and the experimental value obtained in Assembly 1 has not only increased in absolute magnitude but also changed sign. The agreement between the C2 value and the experimental value on the other hand is good. The high C1 value is now mainly caused by the large absorption assumed between 30 and 70 keV.

A comparison of the experimental and computed sample size dependence in Assembly 3 shows that the calculations overestimate the dependence, which is now mainly caused by resonance effects.

On these grounds it cannot be excluded that both sets overestimate the absorption at lower energies and underestimate the inelastic scattering which would be consistent with the reaction-rate measurements in the reflector, and that the self-shielding factors for Cu given by the Bondarenko set are somewhat too low (correct f-values should be closer to 1). Another possible explanation of the discrepancy observed in sample size dependence in Assembly 3 would be that the effects of scattering- and capture-resonances cancel out to a greater extent than calculated.

Ni

The absorption cross section of Ni in the energy range of the flux peak, 200-800 keV, is small, 0.01 b. σ_c rises slowly towards lower energies but $\sigma(n,p)$ increases rapidly above 800 keV. The reactivity properties of Ni in the spectra examined here are about the same as those of Cu.

The experimental result in Assembly 1 (Table 4) gives a slightly smaller reactivity coefficient than the computed values. When comparing the two calculated coefficients it should be remembered that the cross section sets used are both weighted with a fission spectrum above 2.5 MeV, where most of the absorption and inelastic scattering occurs.

In Assembly 3 a relatively large discrepancy between the experimental value and the computed C1 value was noticed. The C2 value reproduces the spectrum shift satisfactorily, and the small absolute discrepancy may now depend on flux weighting. An examination of the data leading to the high C1 value revealed that σ_c in the Häggblom set is on the average twice as high as the Bondarenko value in the energy range 10 keV - 100 keV. As the flux level in this range has greatly increased in Assembly 3, this difference seems to explain the high C1 value.

5.4 _ Weak_absorbers

Z r

Zirconium is a weak absorber with an absorption cross section which is about 0.01 b above 100 keV. The reactivity coefficient of Zr is thus sensitive to the shape of the adjoint spectrum. The inelastic cross sections used in both sets are almost equal, but the Häggblom set erroneously assumes an absorption cross section $\equiv 0$.

An examination of the experimental and calculated values (Table 4) reveals large discrepancies in both assemblies, the experimental values being much more positive than expected. It should be noted that a revised C1 value would be even more negative. It is difficult to explain the large discrepancies as the agreement of the other weak absorbers has been relatively good, which indicates that the adjoint spectrum is correctly calculated.

As mentioned in chapter 3, it is probable that the brass walls and the Al tube slightly deplete the high-energy flux in channel A and, as will be shown in the discussion of the results of the pure scatterers, the anisotropy caused by the experimental arrangement is perhaps stronger than the TDC calculations indicate. Both of these error sources tend to make the experimental coefficients more positive than the calculated. But the question remains why only the Zr coefficient is affected to such an extent.

In most cases the Zr measurements performed with different ZPR-III assemblies, including assemblies with similar compositions to our Assemblies 1 and 3, have shown a qualitative agreement between calculations and experiment [7]. But in Assemblies 23 and 32

the Zr measurements have shown large discrepancies of the same sign as those reported here. Assembly 23 was an Al-diluted and Assembly 32 a steel-diluted system. Although these compositions are very different from those of FR0, the real spectra in Assembly 1 and in the two ZPR-III systems mentioned are rather similar but, because of the absence of U238, the adjoint spectra in Assemblies 23 and 32 are almost constant at higher energies. It is thus not possible directly to compare the discrepancies.

Fe

Iron is a weaker absorber than Cu and Ni in the energy range of interest here. σ_c is only a few mb above 10 keV. The negative reactivity effect caused by inelastic scattering thus tends to overshadow the absorption effect.

Table 4 shows certain deviations between the experimental and calculated values in Assembly 1. The experimental value is slightly higher than the calculated C2 value, while the C1 set gives a still less negative reactivity coefficient.

An examination of the values in Assembly 3 shows that the discrepancies persist qualitatively but are now smaller. On the basis of these results it seems that the cross sections used slightly underestimate the inelastic scattering. A comparison of the effective cross sections in Table 6 reveals how the net effect of scattering has become less negative between Assemblies 1 and 3.

The sample size dependence has been measured in both Assemblies 1 and 3. The experimental results have been satisfactorily reproduced by calculations (Table 5, Fig. 10b and Fig. 11b). The resonance shielding and the group flux perturbations contribute about equal amounts to the calculated sample size dependence.

Cr

σ_c of chromium rises from about 0.004 b at 1 MeV to about 0.02 b at 10 keV, and inelastic scattering is again mainly responsible for the negative effective cross section.

An examination of the experimental and calculated values in Assembly 1 (Table 4) reveals small deviations, and especially Bondarenko seems to give a somewhat too negative coefficient.

In the energy group 1.4-2.5 MeV Bondarenko, mainly because of the absence of weighting, gives a much larger inelastic group cross section than the Häggblom set - to some extent this is true also above 2.5 MeV although both sets are similarly weighted in this range. On the other hand, above 500 keV the Häggblom set assumes significantly larger absorption cross sections than Bondarenko. The approximate equality of the calculated values is thus rather the result of cancelling effects.

The small discrepancies between calculated and experimental values essentially remain in Assembly 3. On the basis of these results it is difficult to say whether the absorption cross sections or the inelastic cross sections cause the deviations. The effective cross sections in Assemblies 1 and 3 show that the decrease of the negative reactivity contribution, due to inelastic scattering between 1 and 3, is more important than the increase of the absorption.

Ti, V

Titanium and vanadium have only been examined in Assembly 1. For both materials only Bondarenko group cross sections are available.

Ti, like Cr, is a very weak absorber. Between 200 keV and 2 MeV σ_c is only a few millibarns. The down-scattering thus essentially determines the reactivity coefficient and possible errors in the inelastic cross sections used are important. A comparison of the experimental and calculated values (Table 4) shows a relatively good agreement for Ti. As the inelastic scattering mainly occurs from energies above 2.5 MeV, it is possible that approximately correct cross sections are obtained due to the realistic weighting function used in this range.

The absorption in V in Assembly 1 may also be virtually disregarded as σ_c around the flux peak only amounts to 1-2 mb. Inelastic scattering again gives the negative effective cross section. A comparison of the experimental and calculated values in Table 4 reveals a strong discrepancy, the experimental coefficient being significantly less negative than the calculated. An examination of the inelastic cross sections, however, shows that V, contrary to Ti, has large inelastic cross sections below 2.5 MeV, where the group cross sections in Bondarenko are lethargy averages. The negative effect of the inelastic scattering from energies between 800 keV and 2.5 MeV will thus be

strongly overestimated and will give a too high negative reactivity coefficient. It should also be noted that the elastic group cross sections of V are considerably higher than those of Ti below the minimum of the adjoint spectrum, while both materials have about equal σ_{el} above 800 keV.

5.5 Scatterers

Al

Aluminium is a pure scatterer with an almost negligible absorption cross section. The elastic scattering below 1 MeV gives a positive reactivity contribution, but because of the rapidly increasing adjoint spectrum above 1 MeV the positive effect is cancelled by inelastic and elastic scattering from energies above the adjoint minimum. In this way the small absorption cross section is decisive and gives a slight negative coefficient in these spectra.

The scattering cross sections used in the two sets are approximately identical but the absorption cross sections are rather different. The Häggblom set assumes a relatively high capture cross section, about 0.01 b, above 800 keV and $\sigma_c \equiv 0$ below this energy. This does not seem entirely adequate. The σ_c given by Bondarenko are, on the other hand, a few mb in the whole range 10 keV - 4 MeV. The influence of these differences is clearly seen in the change of the calculated values between Assemblies 1 and 3. The agreement between experimental and calculated values (Table 4) is acceptable for the sample Al-1.

Some measurements of the reactivity coefficient as a function of sample size were performed in Assembly 1 with channel B. The results reveal that the acceptable agreement obtained for Al-1 was perhaps only fortuitous. Table 5 and Fig. 12a show that the reactivity coefficient is strongly dependent upon sample size. The experimental dependence is moreover opposite in sign to that given by calculations and to the dependence that might intuitively be expected.

As a qualitative agreement has been obtained for other weak absorbers, except for Zr, it seems improbable that the adjoint spectrum is altogether erroneously calculated. Nor is it probable that the shielding of the scattering resonances below 1 MeV is underestimated, as this same curious sample size dependence has been measured also with C samples.

It is possible that the sample size effect depends on the flux ani-
sotropy caused by the experimental arrangement. Although the regular
and adjoint angular fluxes in channel B were obtained with two-dimen-
sional S_N calculations, it seems that the fluxes, combined in the
PERCYL code with the assumption of isotropic scattering, cannot re-
produce correctly the perturbation effect caused by pure scattering
in the chambers.

It is possible to obtain the calculated reactivity effect caused
by scattering within the energy groups by computing the reactivity
coefficient on the basis of the total (only space and energy dependent)
fluxes, which are then assumed to be isotropic, and by using the cal-
culated angular fluxes in the same points. As an average along the
central axis in Assembly 1 in the sample chamber B we obtain
- 0.036 pcm/g in the former case and - 0.021 pcm/g in the latter. The
difference is thus due to the calculated anisotropy. The experiments,
however, seem to indicate that the effect is much more important.

C

Carbon has a completely negligible absorption cross section and
the reactivity coefficient is thus extremely sensitive to the shape of
the adjoint spectrum. In contrast to Al, carbon has a non-zero in-
elastic cross section only at such high energies that it may safely be
disregarded in these qualitative discussions.

For the pure scatterers the comparison of the experimental and
calculated values is complicated by the fact that two different forms
of code have been used, i.e. the diffusion-theoretical code MUCC and
the transport-theoretical S_N codes. For most materials the central
reactivity coefficients obtained with the two different codes, using the
same cross sections have proved to be almost identical. But for Al, O
and C, the MUCC code tends to give coefficients which are approximate-
ly 10 % more positive than those given by the S_N fluxes, although the dif-
ferences in calculated group fluxes are very small, less than 1 %.

The agreement between the experimental and calculated values is
relatively good for the sample C-1 in both Assemblies 1 and 3 (Table 4).
The absence of inelastic scattering has resulted in a strongly positive
coefficient. Although less scattering occurs from energies above 1 MeV

in Assembly 3 than in Assembly 1, the effective cross section has not increased (Table 6). This is probably due to the fact that a greater part of the scattering in Assembly 3 occurs below 200-300 keV, where the slope of the adjoint spectrum in both assemblies is slightly smaller than above 300 keV, and on the fact that the slope below 1 MeV is on the whole slightly smaller in Assembly 3 than in 1 (Fig. 5).

The sample size dependence of the reactivity coefficient has been measured in both Assemblies 1 and 3 (Table 5 and Fig. 12b). As mentioned earlier, an anomalous sample size dependence which may be due to the experimental arrangement was found also for C in Assembly 1. The reactivity coefficient rises with decreasing sample size from + 0.15 pcm/g to + 0.23 pcm/g, and it has not sofar been possible to reproduce this effect by calculations.

In Assembly 3 the expected sample size dependence was measured. The reactivity coefficient rises slightly for larger samples, because of less scattering from energies above 1 MeV. It is possible that the anisotropy caused by the experimental arrangement is less in Assembly 3 than in 1, but it seems odd that the effect has now completely vanished.

O

Oxygen may be regarded as a pure elastic scatterer. An attempt to measure the reactivity coefficient of oxygen was made with CuO; but because of the strong sample size dependence of elastic scatterers that was encountered the results should be analyzed keeping in mind that the oxygen coefficient is probably rather size-dependent.

The large differences occurring between the calculated values (Table 4) again depend mainly on weighting and on the group number, as the cross sections used are almost identical. To some extent the high C2 values are also due to the use of diffusion-theoretical fluxes as explained above. It thus seems probable that the large discrepancies between calculated and experimental values cannot be attributed to any large errors in the oxygen cross sections or in the calculated adjoint spectra. Even disregarding the possible anisotropy as a cause of the anomalous sample size dependence, the results indicate that the central reactivities of pure elastic scatterers should be analyzed with some suspicion as the calculated values are extremely sensitive to the perturbation methods used.

An examination of the values in Assemblies 1 and 3 shows that the calculated and experimental values are affected by the spectrum shift in the same way qualitatively. As for C, the graphite dilution decreases the effective cross section.

5.6 _ Boron

The results obtained in the boron measurements deviate to some extent from the results given by the heavy absorbers. The measurements have been performed with natural boron as a function of sample size, and with a small sample of enriched boron (Table 4).

The computed values for Assembly 1 will be considered first. The large difference between the values is mainly dependent on different capture cross sections at higher energies, as the Häggblom set assumes σ_c values which are much larger than the values given by Bondarenko above 800 keV. As the absorption at higher energies somewhat loses in significance, and the absorption below the flux maximum increases, the change of the computed values in relative magnitude between the two assemblies is easily explained.

The experimental values show a slightly smaller spectrum degradation between the two assemblies than expected. This is not consistent with the results obtained with the heavy absorbers, which indicated correctly calculated low-energy fluxes. It is, however, necessary to make a critical revision of the boron cross sections in the Häggblom set before any definite conclusions can be drawn.

The dependence on sample size may at first sight seem strange, but is due to the fact that scattering down to a certain energy level below the flux maximum level more than compensates the absorption at this level, as the flux decreases rapidly down the energy scale.

The results obtained with enriched boron are consistent with the natural boron results. Unfortunately cross sections only for natural boron are at present available in the Häggblom set.

5.7 _ Strongly moderating materials

D, H

D and H are heavily moderating materials. The elastic down-scattering now transfers neutrons over many groups. It should be pointed

out that the mathematical methods used are not really adequate for these materials. The flux perturbations in the lower energy groups reach such a magnitude that the whole perturbation approach is invalidated. No close agreement between experimental and calculated values for the finite samples can be expected for these materials.

The differences between the calculated values of heavy water depend on different weightings and on the varying number of groups, as the cross sections used for deuterium are almost identical. The C2 values again somewhat overestimate the down-scattering compared to the C1 values. The experimental value obtained in Assembly 1 (Table 4) lies between the calculated values, but the perturbation model used seems to have lost its validity in Assembly 3 as the experimental value is now significantly above both calculated values. The fact that the effective cross section is lower in Assembly 3 may again be explained by the details of the adjoint spectra.

Diphenyl, $C_6H_5-C_6H_5$, was tested in channel A with three different samples in Assembly 1 and with two in Assembly 3. The results are given in Table 4 and the sample size dependence is illustrated in Figs. 13a and 13b. An examination of the values obtained by extrapolation to zero sample size in Assembly 1 shows that Bondarenko overestimates the down-scattering, while set 2 gives a relatively correct value. The cross sections used for hydrogen are almost identical in both sets. All calculated values, however, fail to give an acceptable sample size dependence.

Even the value obtained with the smaller sample in Assembly 3 is significantly larger than the calculated values, but extrapolation to zero sample size probably gives acceptable agreement.

6.   Some complementary measurements

6.1 _Foil activations

Some foil activations were made in Assembly 3 with channel B in an effort to check the calculated flux perturbations. It should be emphasized, however, that no thorough and penetrating experimental study of the real and adjoint flux distributions in the samples and in an empty

sample chamber was made to supplement the central reactivity meas-
urements. If the measurements are to be continued, it seems important
to do this.

The foil activations reported here measure only the relative ra-
dial distribution. The activations were performed along the central
vertical axis in an empty chamber and in two chambers containing the
samples C-2 and Fe-2, respectively. These samples fill one half of
a sample chamber. It should be noted that the samples are much larger
than those generally used in the central reactivity measurements. The
reactions studied are given in Table 7.

Table 7

Reaction	Measured activity		Half life
In115(n, n')	γ	0.335 MeV	4.5 h
Au197(n, γ)	β		2.7 d

The In reaction has an effective threshold at 1.5 MeV while the
Au reaction is approximately a 1/v detector. The foils were irradiated
for two hours at a power level of about 10 Watts. The experimental
techniques used to analyze the data are described in [3].

The results are shown in Figs. 14 and 15. The TDC fluxes avail-
able with channel B were used to obtain calculated reaction rate distribu-
tions in an empty chamber, and with the perturbed fluxes computed by
the PERCYL code calculated reaction rate distributions were obtained
in the chambers which contained samples. The values have been norm-
lized, so that the calculated and experimental values at the lower end
of an empty sample chamber coincide. All the four curves in each figure
are directly comparable, as only this normalization was done. This is
not an ideal normalization because of the steel present below the sample
chamber (Fig. 2), but with the data available it was the best possible.
Before starting on a comparison of experiments and calculations it should
also be remembered that the foils have a finite size (about 1 cm^2), while
the calculated fluxes refer to the central vertical axis, and that the exp-
erimental and statistical uncertainties together give errors which are
probably about $\pm$ 0.5 %.

The experimental distribution of the In reaction in an empty sample chamber has been qualitatively reproduced by calculations, the dips caused by the steel below the chamber and by the solid Cu bar above being clearly seen. But is obvious that the variations in high-energy flux across the chamber are more pronounced than expected; the ratio between the maximum and minimum experimental values is about 1.15 and the corresponding calculated value is only about 1.09.

The experimental distribution of the In reaction in the carbon and iron samples has been fairly well reproduced by calculations, but because of the existing discrepancies for an empty chamber the agreement is probably to some extent fortuitous. The experiments clearly show how the high-energy flux is decreased rapidly by inelastic scattering in Fe while the elastic scattering in C does not perturb the flux in the MeV region by equal amounts.

The experimental distribution of the Au reaction in an empty chamber has also been qualitatively reproduced by calculations but the measured axial dependence is again more pronounced than calculations indicate. The Au reaction rate decreases slowly towards the Cu bar because of the absence of graphite above the chamber.

The experimental distribution of the Au reaction in the graphite sample shows that even the second order perturbation model used cannot handle the flux perturbations in the low-energy range caused by this large sample. As the group fluxes at lower energies, below 10 keV, are altered by the sample to an extent which certainly invalidates perturbation theory in this range, the discrepancy is not surprising.

It is difficult to state anything with certainty about the Au measurements in Fe but, as expected, the low-energy flux is not greatly altered by this sample.

6.2 Plutonium

The procedure adopted for measuring the reactivity equivalence of the Pu sphere was described in 2.1. Because of the different experimental arrangement used, the reactivity amounts cannot be directly compared with the values obtained in channels A and B.

The experimental results are given in Table 8.

Table 8

Label of sample	Assembly 1	Assembly 3
Pu	2.44 ± 0.02 pcm/g	1.63 ± 0.02 pcm/g

Good agreement is obtained as the calculated values fall within the experimental error limits. This agreement is necessary for the correctness of the conversion of reactivity amounts to effective cross sections described earlier.

7. Final conclusions

7.1 Experimental arrangement

The central reactivity measurements should of course be performed in an unperturbed equilibrium spectrum, corresponding to the core composition, in a volume with an isotropic flux and no gradients. In practice this is impossible because of the experimental arrangement necessary; for safety reasons fuel cannot be used to prevent neutron streaming through the experimental channels.

The spectrum perturbation and the flux anisotropy caused by the experimental arrangements will here be examined starting with the spectrum perturbation and taking the experimental results and the TDC calculations into consideration.

Figs. 3 and 4 show the calculated group fluxes Φ_1, $\Phi_5 + \Phi_6$ and the total flux $\sum_{i=1}^{6} \Phi_i$ along the vertical axis in channel B in Assemblies 1 and 3, respectively. The figures show that the variations in total flux level within the chambers are relatively small in both assemblies. But the high-energy flux Φ_1 decreases strongly towards the Cu bar above the chamber and the steel construction below the chamber. This is especially unfortunate as the negative reactivity contribution caused by inelastic scattering, which for many materials in these spectra is decisive for the effective cross section, is mainly dependent on Φ_1. The relative variations of Φ_1 are about the same in both assemblies.

The low-energy flux $\Phi_5 + \Phi_6$ shows small variations in the chambers, but because of the different core compositions the variations of Φ_6 will be of opposite sign in Assemblies 1 and 3.

The few foil activations made in Assembly 3 with channel B (Sect. 6.1) show that the real flux variations are probably more pronounced than expected. This is a serious disadvantage for the analysis of the experimental results.

As mentioned earlier, no flux calculations have so far been made with channel A. In this case there is no perturbing steel below the chamber, but instead the brass wall and the Al tube surrounding the chamber have to be considered. It seems urgent to calculate the effect of these.

Table 9 shows the effect of the calculated spectrum perturbation caused by the experimental channel B on the effective cross sections in Assembly 1. The cross sections have been computed in the core centre of a homogeneous unperturbed cylinder and at a point on the vertical central axis in channel B, 6.15 cm above the lower end of the chamber. The calculations are of first order and thus relate to infinitesimally small samples. The anisotropy has not yet been taken into consideration. The same effective cross section for Pu239 has been assumed in both cases.

Table 9

Material	Homogeneous assembly	Assembly with channel B
Fe	- 22 mb	- 19 mb
C	+ 11 "	+ 15 "
Natural boron	- 187 "	- 192 "

The differences are not negligible. In future reactivity measurements these perturbations must be mastered, either by comparing different calculated and measured reaction rates in the chamber or, which is preferable, by changing the experimental arrangement so as to minimize the perturbation effects.

The experimental arrangement furthermore causes a certain flux anisotropy. The anisotropy has earlier been mentioned as a possible explanation of the anomalous sample-size dependence of elastic scatterers in Assembly 1. Table 10 gives the calculated effective cross sections in channel B for the same materials as above in the same point of the chamber with assumed isotropic fluxes and with the calculated angular fluxes taken into account.

Table 10

Material	Isotropic flux	Angular flux considered
Fe	- 19 mb	- 18 mb
C	+ 15 "	+ 16 "
Natural boron	- 192 "	- 191 "

These calculated effects are much smaller than those caused by the spectrum perturbation. But it is possible that the anisotropy is more erroneously calculated than the spectrum perturbation.

7.2 Reactivity coefficients

The central reactivity measurements seem to show that the regular and adjoint spectra in the core centre are well calculated in Assemblies 1 and 3.

Most of the significant differences between calculated and experimental values probably depend on erroneous group cross sections of the materials examined. Zr, however, presents some peculiarities as the discrepancies are much larger than any slightly erroneous group cross sections could possibly account for. It is possible that the experimental arrangement changes the sign of the Zr coefficient, but it is strange that other similar materials are not affected to a comparable extent.

The sample-size dependence of the reactivity coefficient has for most materials been fairly well reproduced by the second-order perturbation model and the self-shielding coefficients used. The elastic scatterers are an exception, but it is possible that this discrepancy is due to the fact that the calculations cannot adequately reproduce the anisotropy caused by the experimental arrangement.

7.3 Future work

Further analysis of these measurements should concentrate on Zr and the sample-size dependence of elastic scatterers.

Taking the experiences gained into consideration, the most important improvement, with regard to future measurements, is to modify the experimental arrangement so that the flux in the sample chamber is more equivalent to an appropriate equilibrium flux. This seems more urgent than any improved accuracy of the period measurements.

In this report it has been possible to base the conclusions upon the fact that the measured high-energy flux agrees well with calculations. It would be of great value if the flux measurements could be supplemented by measurements of the adjoint spectra. Such measurements could be made e.g. using neutron sources [14]. Future measurements of effective cross sections should also be supplemented by flux measurements in the chambers and in the samples.

With these data available the central reactivity measurements can be used as a reliable way of testing group cross sections.

References

1. AHLIN, Å and LONDEN, S-O,
   AB Atomenergi, Sweden, Internal report (TPM-RFX-270) 1963
   (in Swedish).

2. AHLIN, Å and LONDEN, S-O,
   Perturbation programmes written for the FRO-work. 1965.
   AB Atomenergi, Sweden, Internal report (RFN-207, FFX-29).

3. ANDERSSON, T L,
   To be published as AE-report.

4. ANDERSSON, T L et al.,
   Experimental studies on assemblies 1 and 2 of the fast reactor FRO.
   Part 1. 1965.
   (AE-195).

5. BJÖRKMAN, J,
   RAMSES, a flexible data collecting and recording system for
   nuclear measurements. 1964.
   AB Atomenergi, Sweden, Internal report (SSI-123).

6. BONDARENKO, I I et al.,
   Group constant for nuclear reactor calculations.
   New York, Consultants, 1964.

7. DAVEY, W G,
   A comparison of experimental and calculated prompt neutron life-times
   and central reactivity coefficients in ZPR-III assemblies and their
   relationship to other reactor parameters. 1963.
   (ANL-6682).

8. HANSEN, G E and MAIER, C,
   Perturbation theory of reactivity coefficients for fast-neutron
   critical systems.
   Nucl. Sci. Eng. 8 (1960) 532-42.

9. HELLSTRAND, E et al.,
   Experimental studies on assemblies 1 and 2 of the fast reactor FRO.
   Part 2. 1965. (AE-207).

10. HOLMQVIST, B and WIEDLING, T,
    Inelastic Neutron Scattering Cross Sections of Cu63 and Cu65 in
    the Energy Region 0.7 to 1.4 MeV 1964.
    (AE-150).

11. HÄGGBLOM, H and NYMAN, K,
    AB Atomenergi, Sweden, Internal report (RFN-173, RFR-293) 1964
    (in Swedish).

12.   HÄGGBLOM, H,
      Theoretical work for the fast zero-power reactor FR-0. 1964.
      (AE-194).

13.   TOPPEL, B J,
      Sources of error in reactivity determinations by means of
      asymptotic period measurements.
      Nucl. Sci. Eng. 5 (1959) 88-98.

14.   TUTTLE, R J,
      Neutron-importance measurements in the advanced epithermal
      thorium reactor (AETR) critical experiments.
      Nucl. Sci. Eng. 21 (1965) 451-62.

Appendix 1

Compositions and critical dimensions of Assemblies 1 and 3

| | Volume percentage of material in core | | | | | | | |
	U238	U235	CF_2	C	Fe	Ni	Cr	Void
Assembly 1	70.1	17.6	0.2	-	4.8	0.5	1.2	5.6
Assembly 3	46.8	11.7	0.1	29.3	4.8	0.5	1.2	5.6

Volume percentage of material in reflector:

Cu	Fe	Ni	Cr	Void
88.5	4.8	0.5	1.2	5.0

Critical masses and dimensions:

| | Assembly | |
	1 (Cylinder)	3 (Cylinder)
Crit. mass kg U	364.7	551
kg U235	72.9	110
Core height, cm	30.1	38.7
Equivalent core radius, cm	15.3	20.4
Minimum reflector thickness, cm	34	30

Appendix 2

Energy limits for the 6 and 14 groups used for the cross sections obtained from the Häggblom set.

g	6 groups			14 groups		
1	10.0	- 1.35	MeV	10.0	- 2.25	MeV
2	1.35	- 0.5		2.25	- 1.35	
3	0.5	- 0.18		1.35	- 0.825	
4	180	- 67	keV	0.825	- 0.5	
5	67	- 9.1		0.5	- 0.3	
6	9.1	- 0.12		0.3	- 0.18	
7				0.18	- 0.11	
8				110	- 67	keV
9				67	- 25	
10				25	- 9.1	
11				9.1	- 5.5	
12				5.5	- 2.1	
13				2.1	- 0.5	
14				500	- 120	eV

NATIONAL ACADEMY OF SCIENCES
NATIONAL RESEARCH COUNCIL

DIVISION OF PHYSICAL SCIENCES
COMMITTEE ON NUCLEAR SCIENCE

SUBCOMMITTEE ON
TECHNIQUES FOR THE
DISTRIBUTION OF SCIENTIFIC INFORMATION

K. Way, Director, Nuclear Data Project, *Chairman*

N. B. Gove, Nuclear Data Project, *Secretary*

E. P. Blizard, Editor, *Nuclear Science and Engineering*

E. L. Brady, Chief, Office of Standard Reference Data, NBS

F. Brickwedde, Chairman, Physics Abstracts Committee, AIP

E. J. Brunenkant, Director, Division of Technical Information, AEC

E. U. Condon, Editor, *Reviews of Modern Physics*

J. Marion, Chairman, Subcommittee on Nuclear Structure, NRC

S. Pasternack, Editor, *Physical Review*

R. Pepinsky, Director, Groth Institute of Crystallography

L. Rosen, Los Alamos Scientific Laboratory

A. B. Smith, Secretary, Neutron Cross Section Advisory Group

H. C. Wolfe, Director, Documentation Research Project, AIP

WHAT TO DO WITH SUPPLEMENTARY MATERIAL

(Too Detailed or too Long for Publication with Journal Article)

1. ANY TOPIC, SHEETS OR MICROFILM accompanying paper submitted to ANY JOURNAL. Attach one copy to your article and suggest editor deposit it with: American Documentation Institute, Auxiliary Publication Project, Library of Congress, Washington, D.C. 20036.

   Material must be sent to the Institute by the *editor* with a $2 deposit fee. (In general editors will add this fee to the page-charge bill.) The Library of Congress will give the editor a document number and purchase price to be included in a footnote of the following type:

   $\left\{\begin{array}{l}\text{``This supplementary material}\\ \text{The complete set of tables}\\ \text{The description of chemical procedures}\\ \text{etc.}\end{array}\right\}$ has been

   deposited as Document No. ———— with the ADI Auxiliary Publications Project, Photoduplication Service, Library of Congress, Washington, D.C. 20036. A copy may be secured by citing the Document number and by remitting $ ———— for photoprints or $ ———— for 35-mm microfilm. Advance payment is required. Make checks or money orders payable to: Chief, Photoduplication Service, Library of Congress.''

   Prices

1–10 pages	$1.25 microfilm or photo-copy
11–20 pages	$1.75 microfilm, $2.50 photo-copy
21–30 pages	$2.00 microfilm, $3.75 photo-copy
31–40 pages	$2.25 microfilm, $5.00 photo-copy

2. ANY TOPIC, SHEETS accompanying paper submitted to CANADIAN JOURNAL. Submit complete work, marking parts for which deposition is desired in Depository of Unpublished Data, National Science Library, National Research Council, Ottawa, Canada.

   Deposition should be made by *editors*. Be sure that a footnote is included in the paper noting the deposition and the fact that copies may be obtained on *request*.

3. NEUTRON CROSS SECTION DATA, SHEETS, PUNCHED CARDS, or TAPE. Send material directly to: Sigma Center, Brookhaven National Laboratory, Upton, Long Island, New York 11973, or ENEA Neutron Data Compilation Centre, Boite Postale No. 9, Gif-sur-Yvette (Seine et Oise), France.

   Either center will accept material in sheet, 80-column punched card, paper tape or magnetic tape form; it is available for re-issue in all these forms but preferably as a machine listing or magnetic tape. Material supplied in machine form should be accompanied by a format description. The centers will accept material whether it is to be published immediately or not. In the latter case, the material should be accompanied by a reasonable description of the method, and laboratory reports or preprints prepared at a later date should be sent to the centers with a note to indicate any changes which may have occurred.

   The ENEA Centre will serve the European area, operating in close collaboration with the Brookhaven Sigma Center; the two centers hold identical master files and operate in identical formats. It is hoped that in the future the users will attempt to provide data, if in machine form, in the format adopted by the centers.

4. REPORTS. If supplementary material is already in report form, note this fact in a footnote giving report number, authors, title, distributor, *and* price. Material formerly sold by the Office of Technical Services (OTS) of the Department of Commerce is now handled by the Clearinghouse for Federal Scientific and Technical Information (CFSTI), National Bureau of Standards, Springfield, Virginia 22151.

NATIONAL ACADEMY OF SCIENCES

NATIONAL RESEARCH COUNCIL

DIVISION OF PHYSICAL SCIENCES

COMMITTEE ON NUCLEAR SCIENCE

SUBCOMMITTEE ON
TECHNIQUES FOR THE
DISTRIBUTION OF SCIENTIFIC INFORMATION

2101 CONSTITUTION AVENUE
WASHINGTON, D. C 20418

To Authors, Editors, Project Leaders,
and Scientific Administrators:

Re: Systematic Use of a *Supplementary-Material De-
posit System* for Data too Lengthy for Journal
Articles

All of us engaged in the dissemination of scientific
results realize that many small and large improvements
must be made in techniques for information transmittal
if these are to provide a better match for techniques of
information production. Recently the Committee on Nu-
clear Science of the National Academy of Sciences —
National Research Council established a Subcommittee
on the Techniques for the Distribution of Scientific In-
formation to "evaluate and originate methods of gather-
ing and distributing scientific information on nuclear
physics."

The Subcommittee hopes to make both major and
minor suggestions for improvements in information trans-
mittal. One minor suggestion concerns the need for
more orderly handling of material which may be con-
sidered as supplementary to journal articles, such as
the numerical data on which graphs are based.

The need is especially acute in the area of nuclear
cross sections where numerical values are needed for
many calculations and programs. Countless hours are
spent, at present, by readers in efforts to extract nu-
merical values from curves — hours which could be
saved if a simple means for securing the tabular data
were available. (A letter to the authors proves not to
be a simple means a few years, or even a few months,
after publication.)
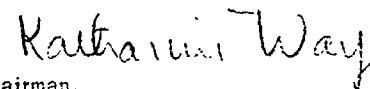
For data basic to graphs, and for all other material
which is too detailed or too long for journal publication,
the Subcommittee urges the wide adoption of a *supple-
mentary-material deposit system.*

Suitable depositories already exist: for general ma-
terial, the American Documentation Institute Auxiliary
Publications Project at the Library of Congress in
Washington and the Depository of Unpublished Data of
the National Research Council in Ottawa; for neutron
cross sections, the Brookhaven Sigma Center and the
ENEA Neutron Data Compilation Centre, Saclay.

An important part of the *supplementary-material de-
posit system* is a clear notice in the published paper
about the existence of the material, the method of secur-
ing copies, and the price. Complete details concerning
existing mechanisms are given in this flyer which we
urge be distributed as widely as possible. Additional
copies are available from the Subcommittee.

Consistent recourse to a *supplementary-material de-
posit system* can shorten many journal articles and intro-
duce considerably more order into the information flow.
Please help by calling the attention of others to the
benefits of such a system and the mechanisms for putting
it to use.

Sincerely yours,

Katharine Way

Chairman,
Subcommittee on Techniques for the
Distribution of Scientific Information

August 17, 1965
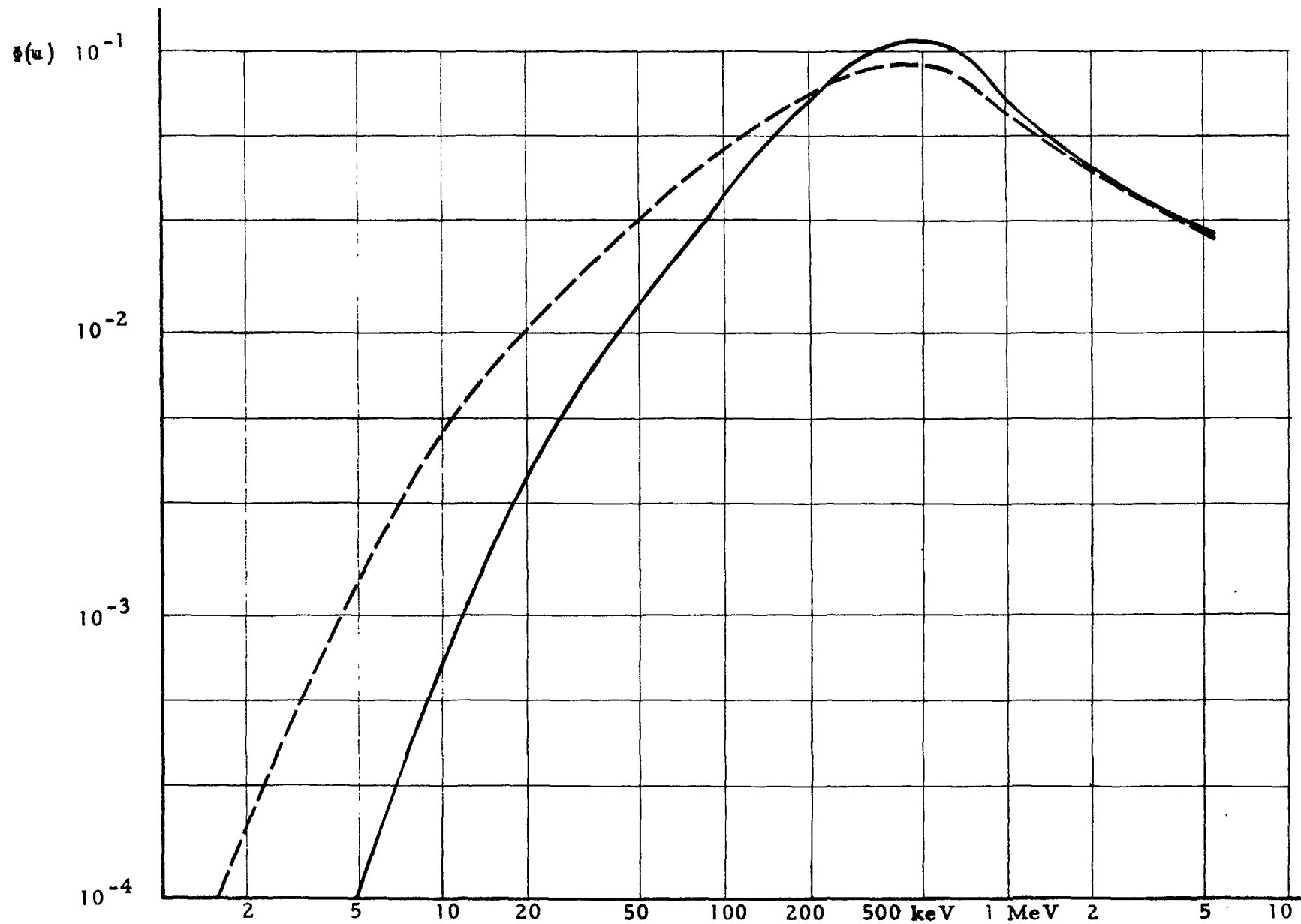
Fig. 1

The regular fluxes per unit lethargy at the core centre of Assemblies 1
and 3 as obtained by 14-group S_N calculations

Full line = Assembly 1   Dotted line = Assembly 3
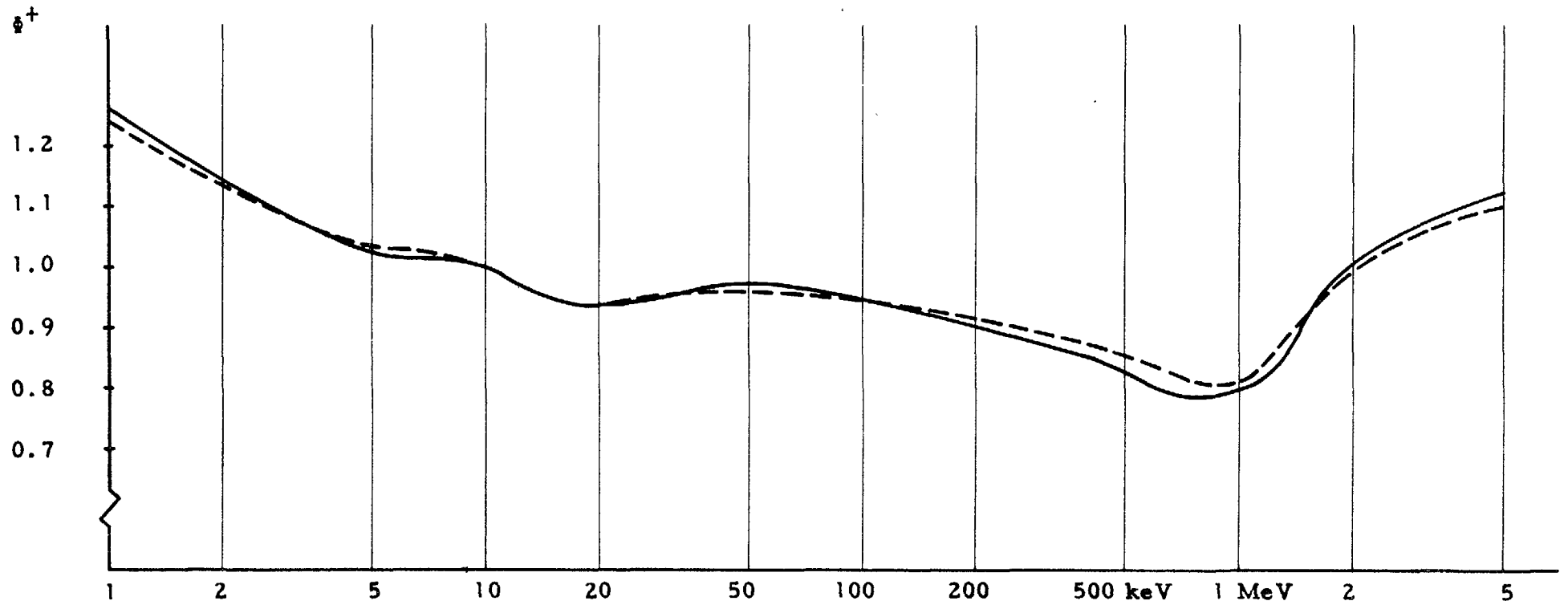
Fig. 2

The adjoint spectra at the core centre of Assemblies 1 and 3 as obtained by 14-group S_N calculations

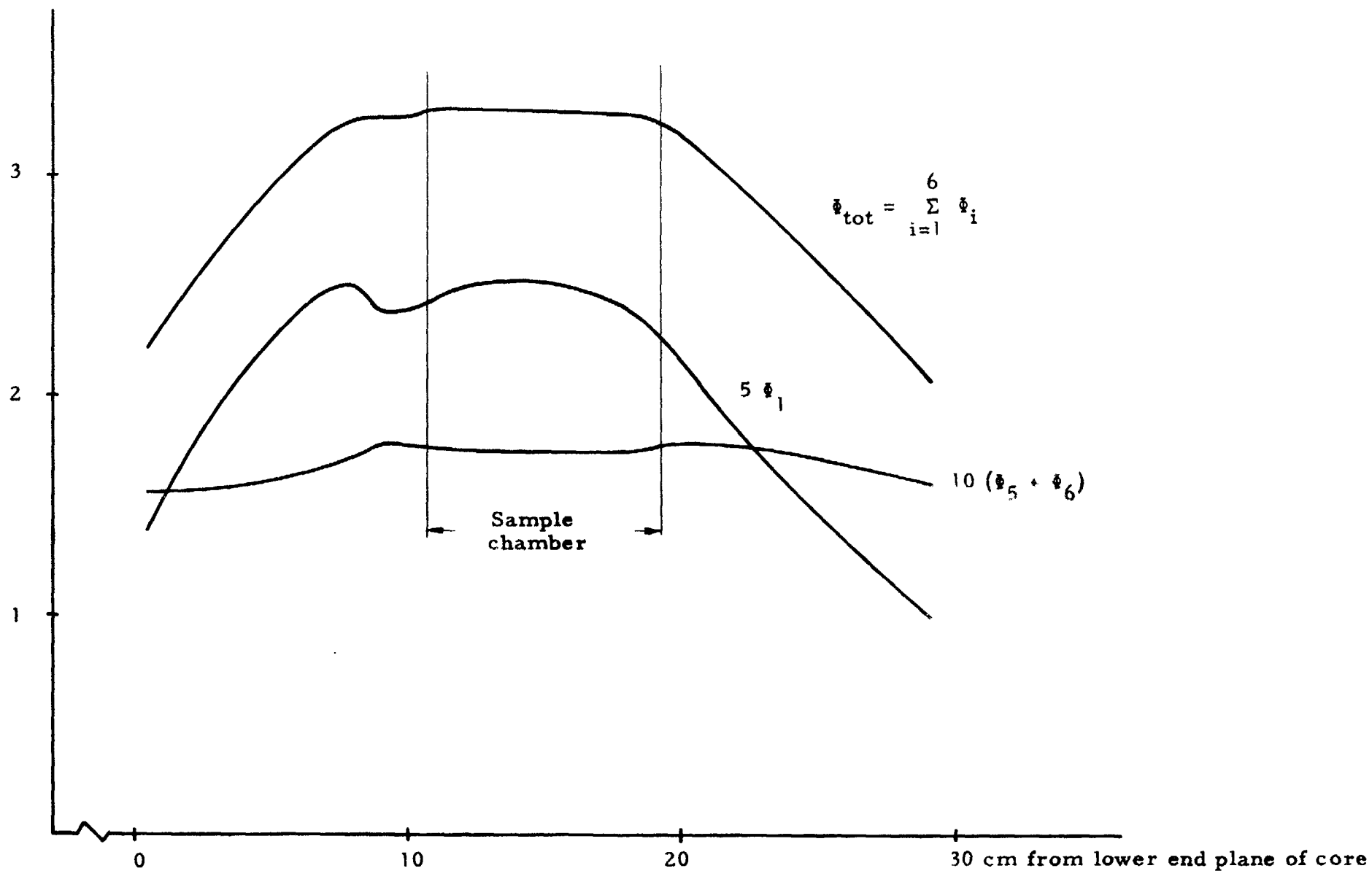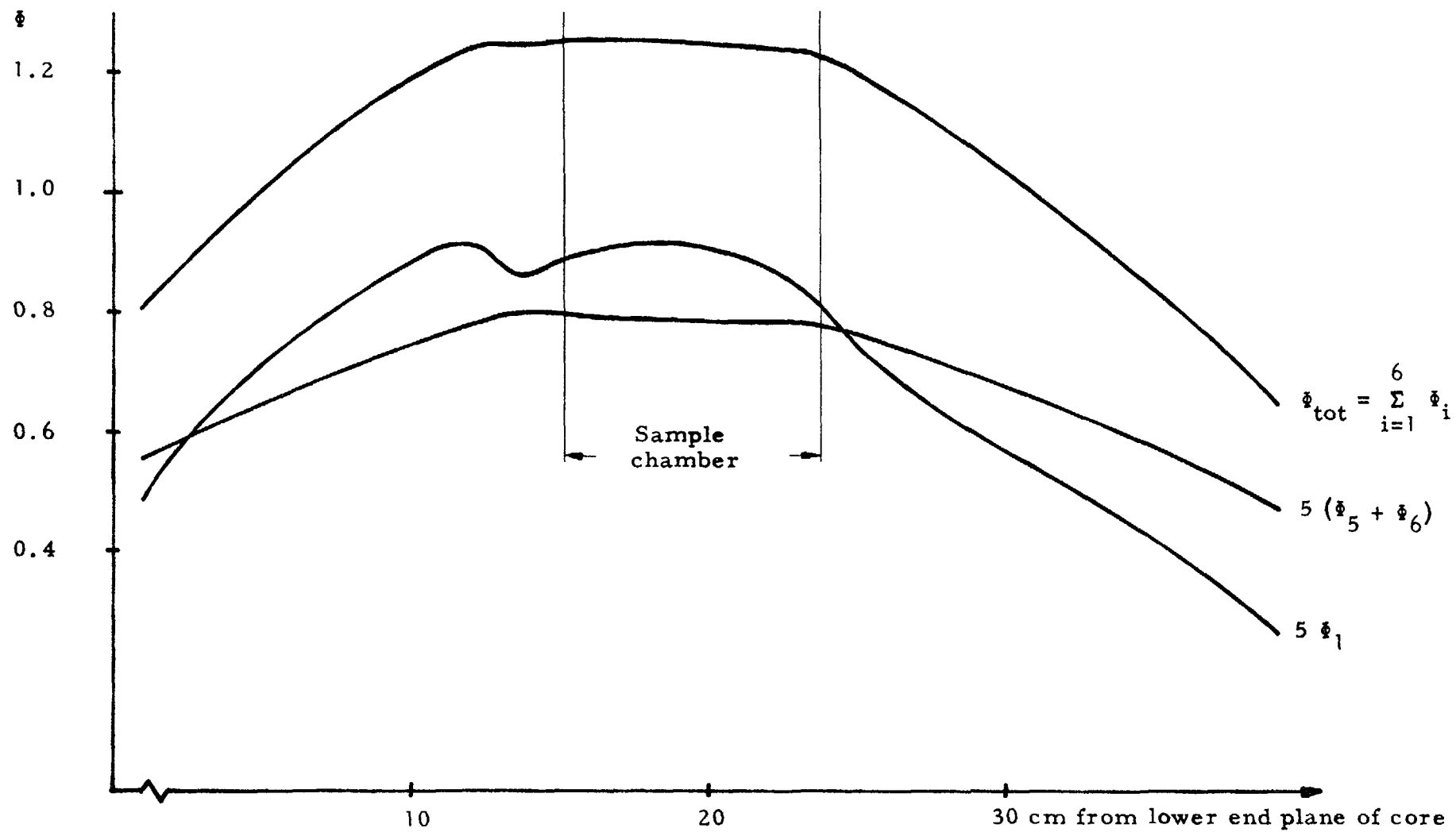Full line = Assembly 1   Dotted line = Assembly 3

Fig. 3

Calculated regular group fluxes along the central vertical axis in Assembly I with experimental channel B
and an empty sample chamber as obtained by a 6-group TDC calculation

Fig. 4

Calculated regular group fluxes along the central vertical axis in Assembly 3 with experimental channel B
and an empty sample chamber as obtained by a 6-group TDC calculation

SCALE 1:10

SAMPLE CHAMBER

SAMPLE CHAMBER AND CHANNEL
NOT TO SCALE

SOLID BRASS
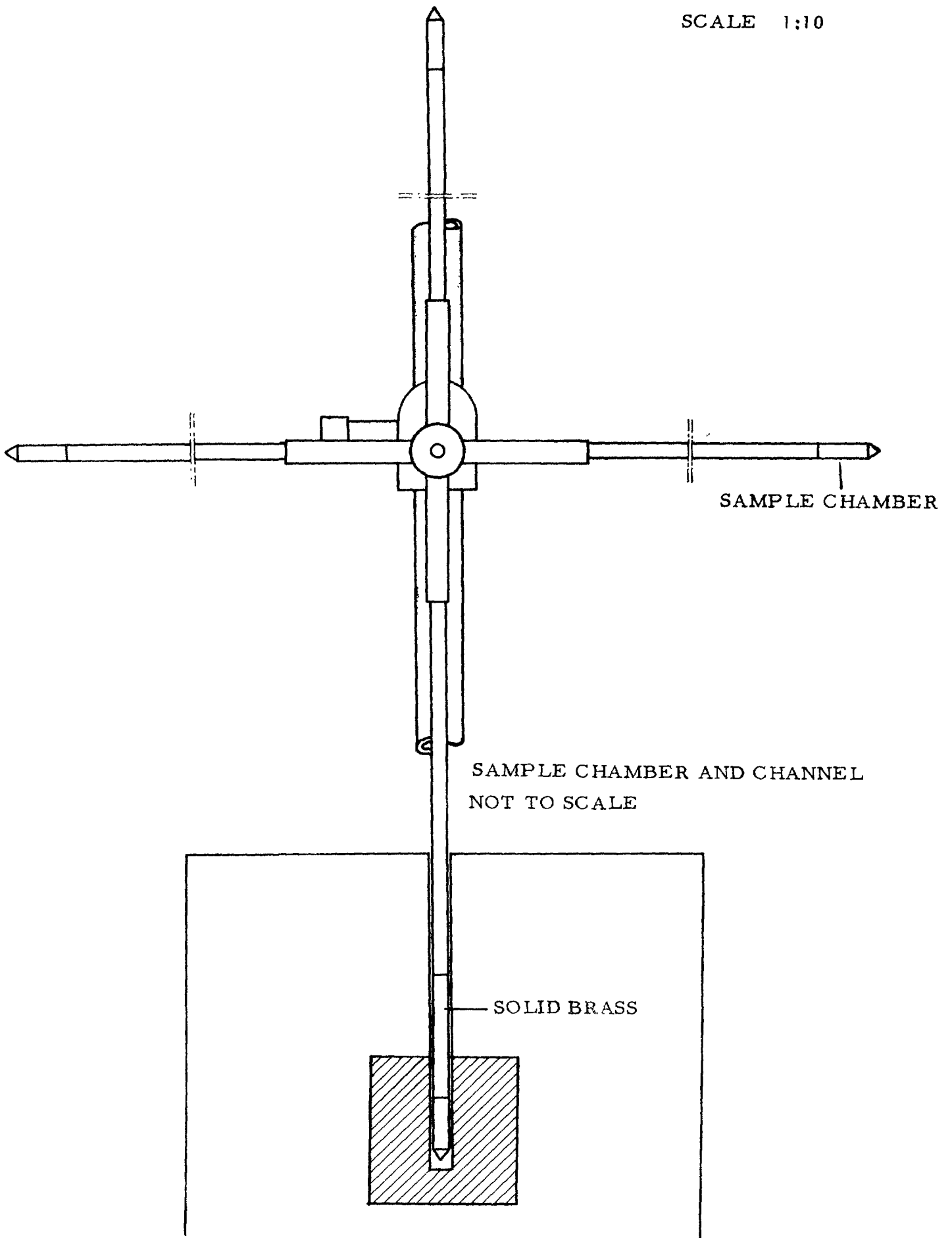
Fig. 5

Experimental arrangement with channel A

cm

15

10

5

0

5

10

15

Aluminium tube

REFLECTOR

Brass bar

CORE

Sample chamber

Brass walls

0   5   10   15   cm
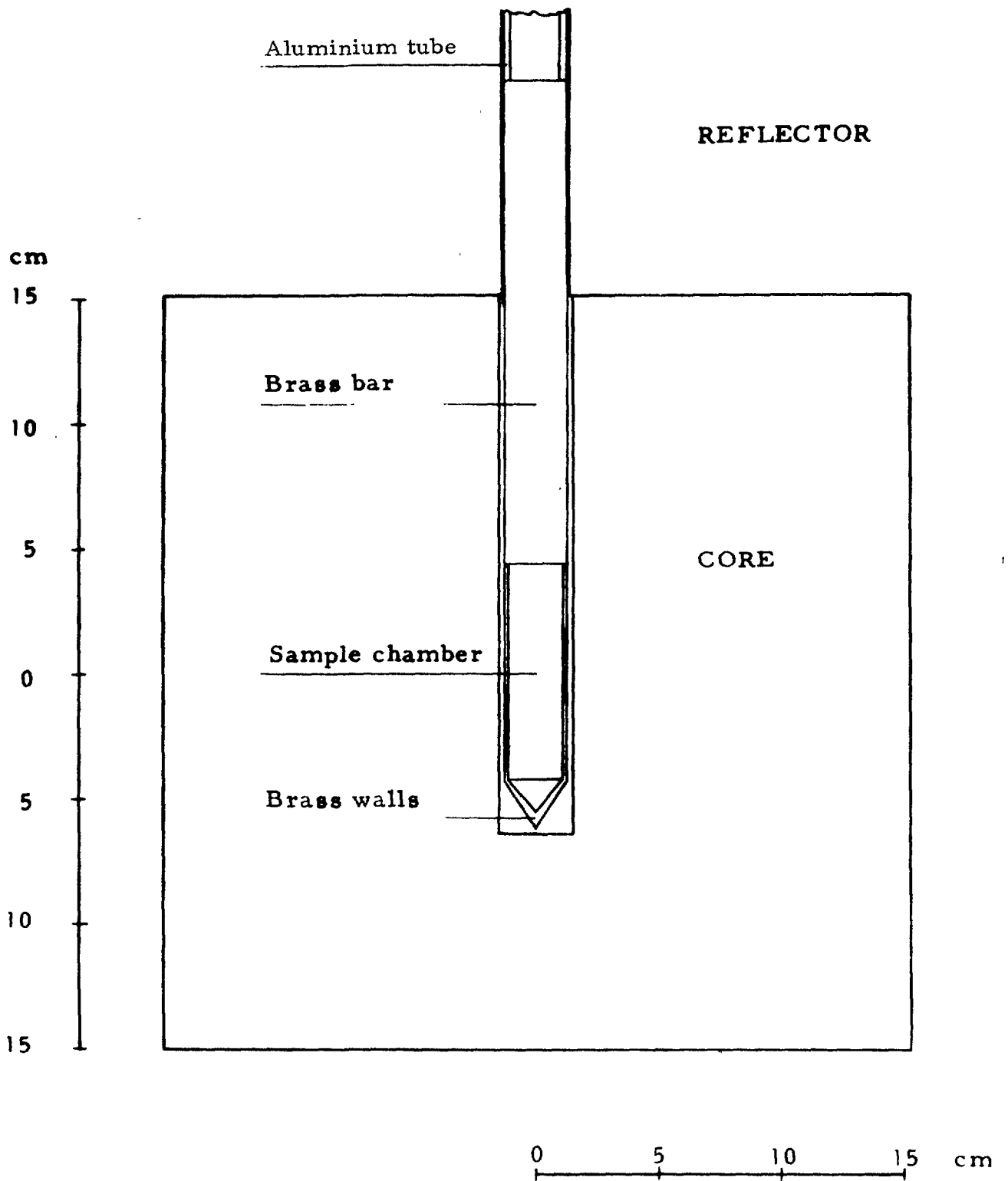
Fig. 6

Schematic vertical section through Assembly 1
with experimental channel A

Fig. 7

Schematic vertical section through Assembly 1
with experimental channel B

Steel frame

Copper tubes

Aluminium tube

Chamber walls

Fuel plates
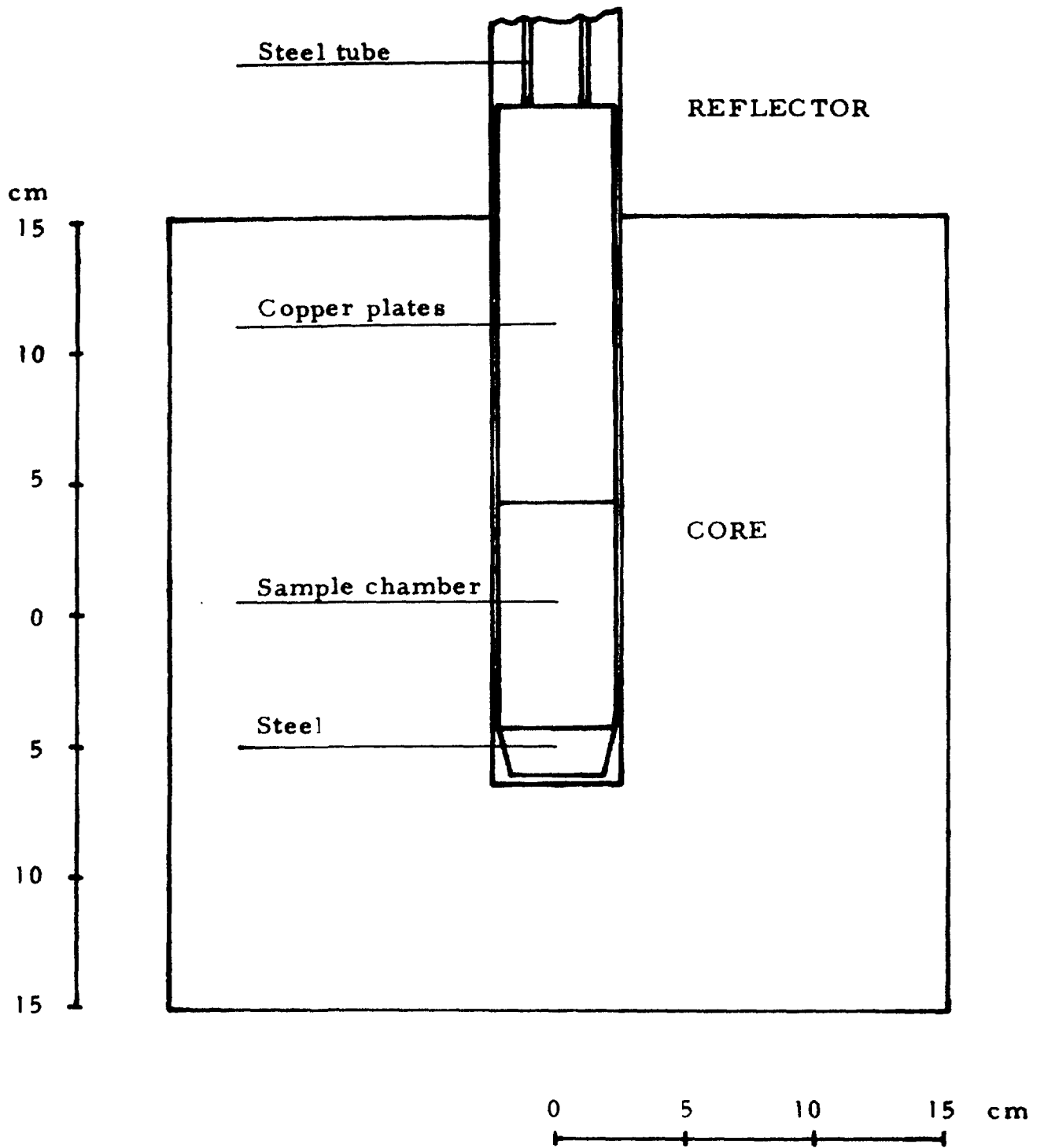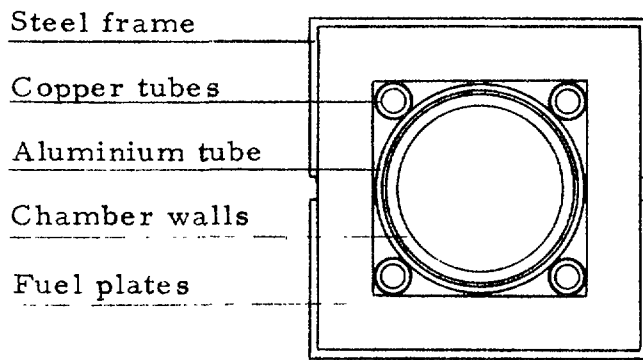
Fig. 8 a

Horizontal section at the centre plane through the central fuel
element with experimental channel A

Steel frame

Steel ring
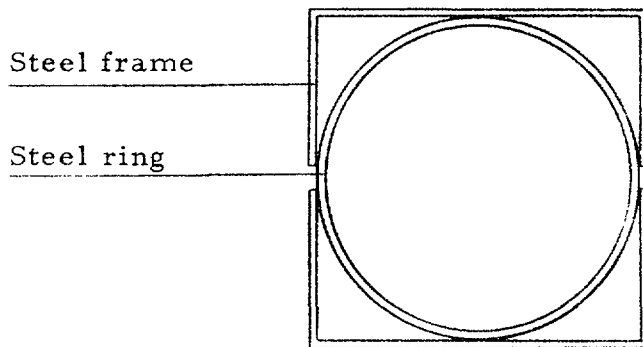
Fig. 8 b

Horizontal section at the centre plane through the central fuel
element with experimental channel B
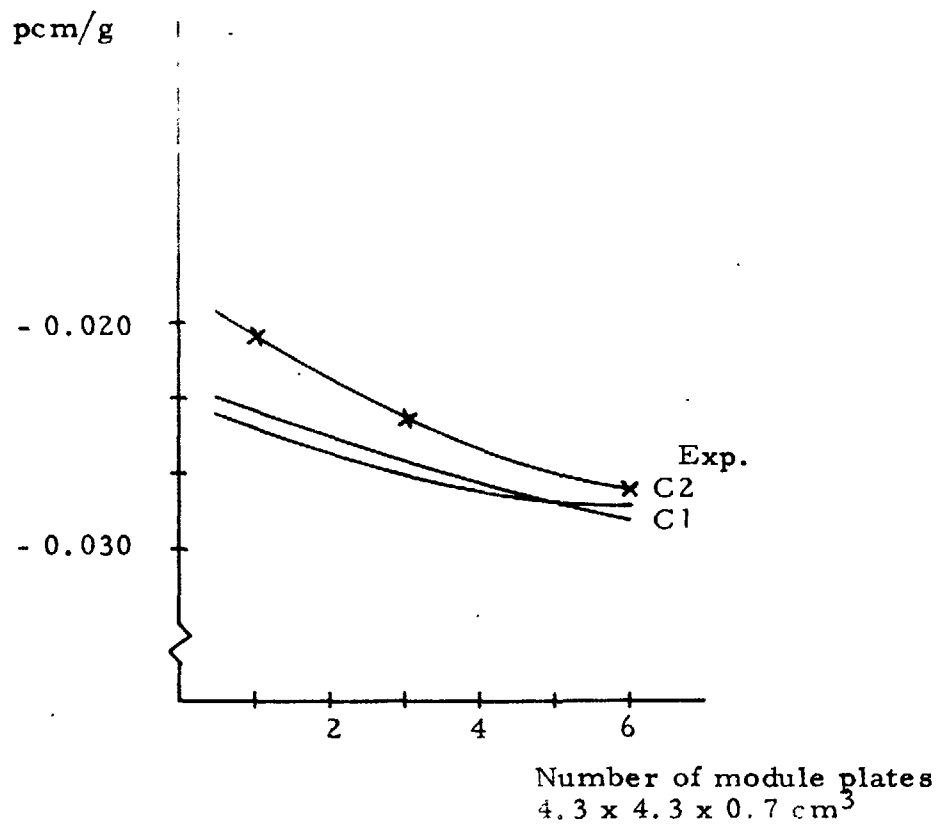
Fig. 9 a

Sample size dependence of reactivity coefficient
of natural uranium in Assembly 1
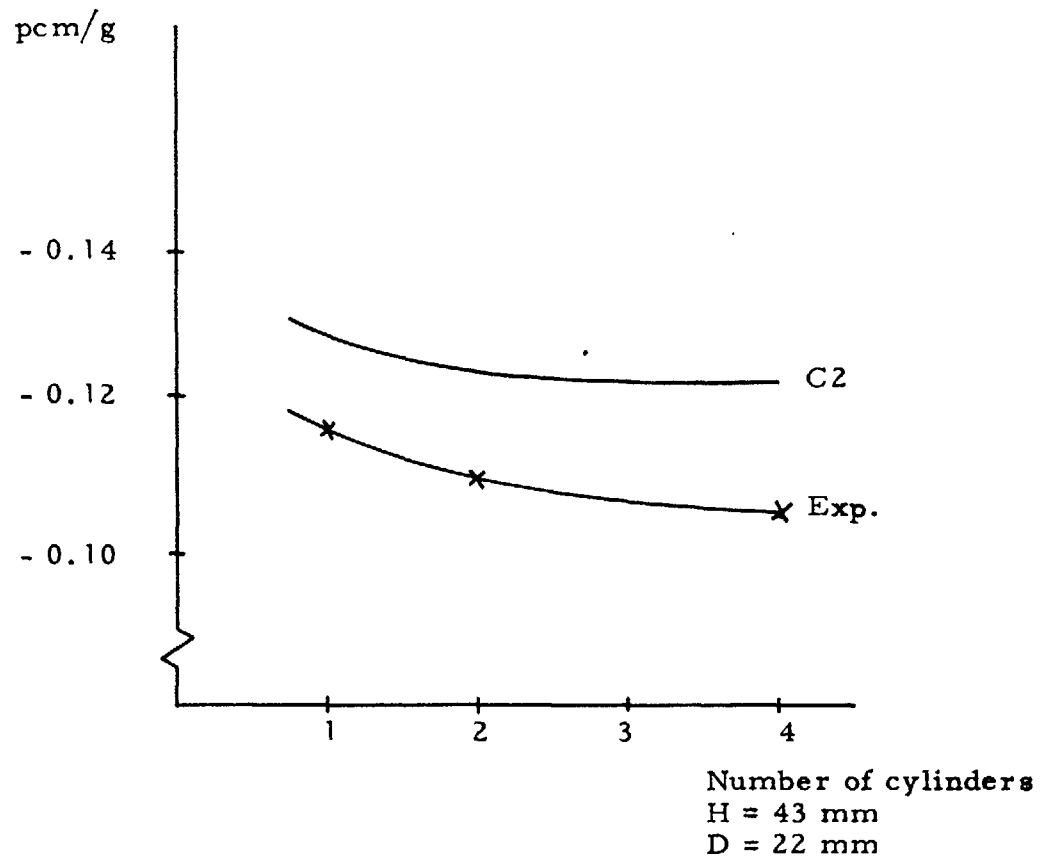
Fig. 9 b

Sample size dependence of reactivity coefficient
of thorium in Assembly 1
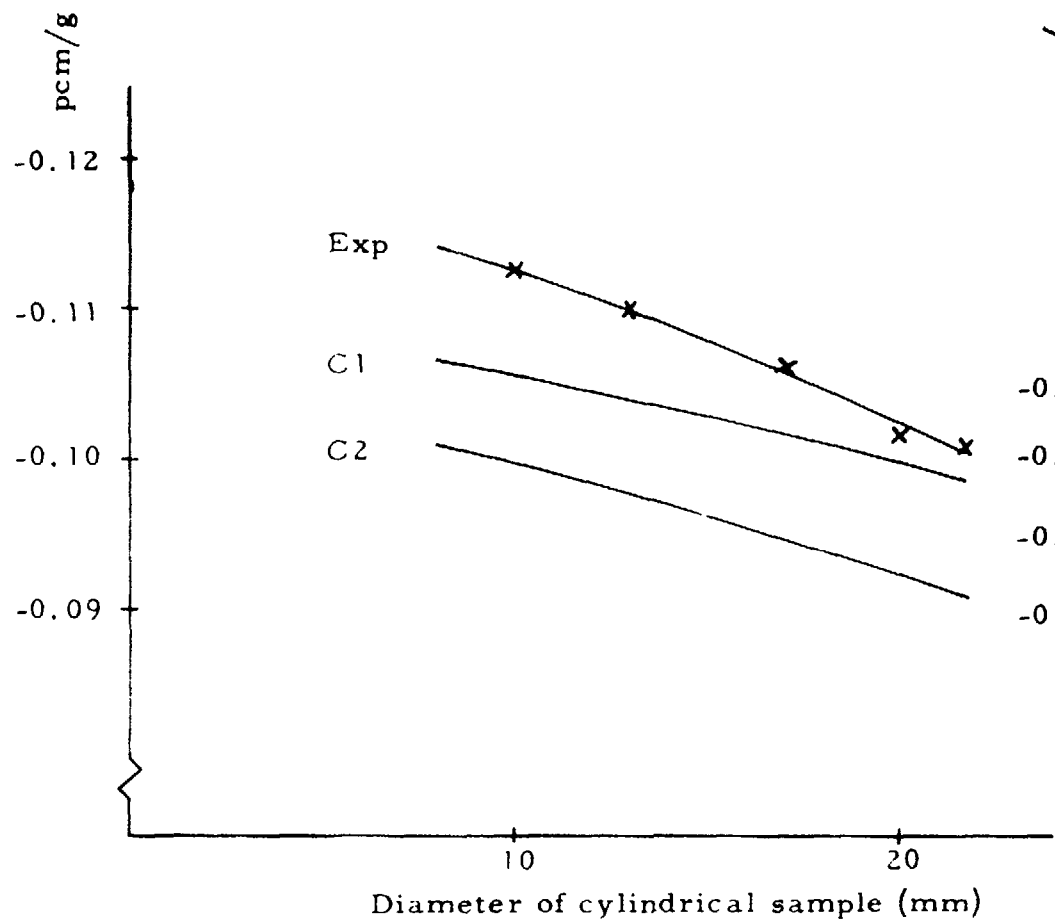
Fig. 10a

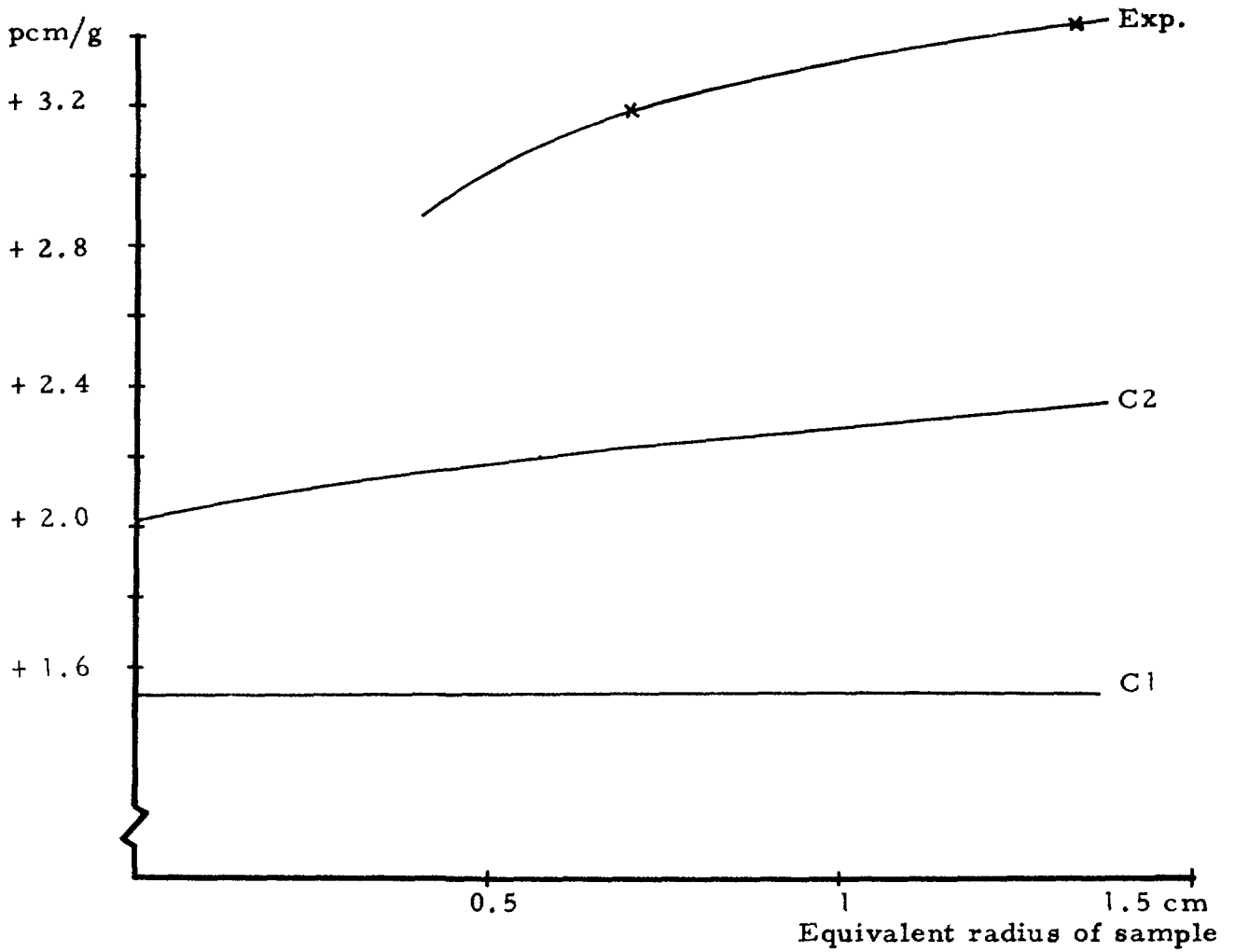Sample size dependence of reactivity
coefficient of copper in Assembly 1
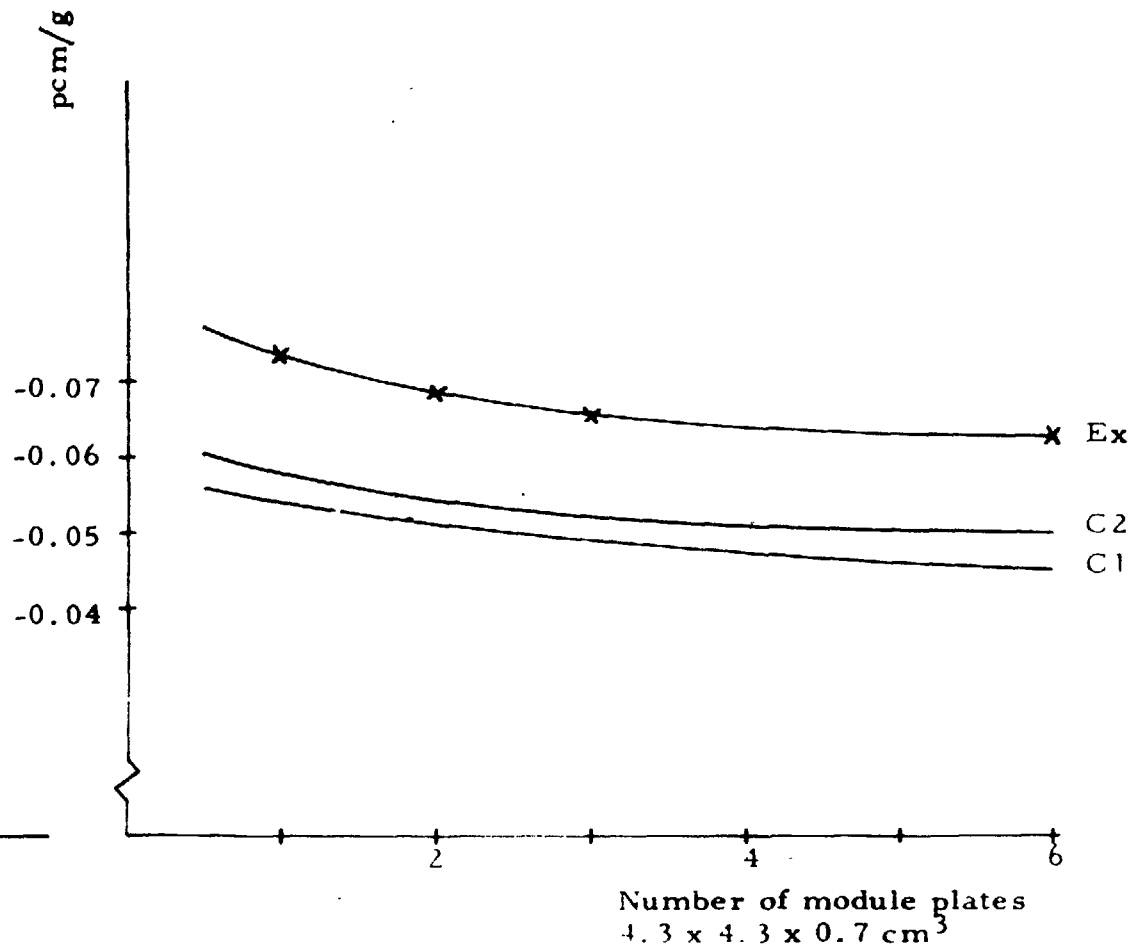
Fig. 10b

Sample size dependence of reactivity
coefficient of iron in Assembly 1
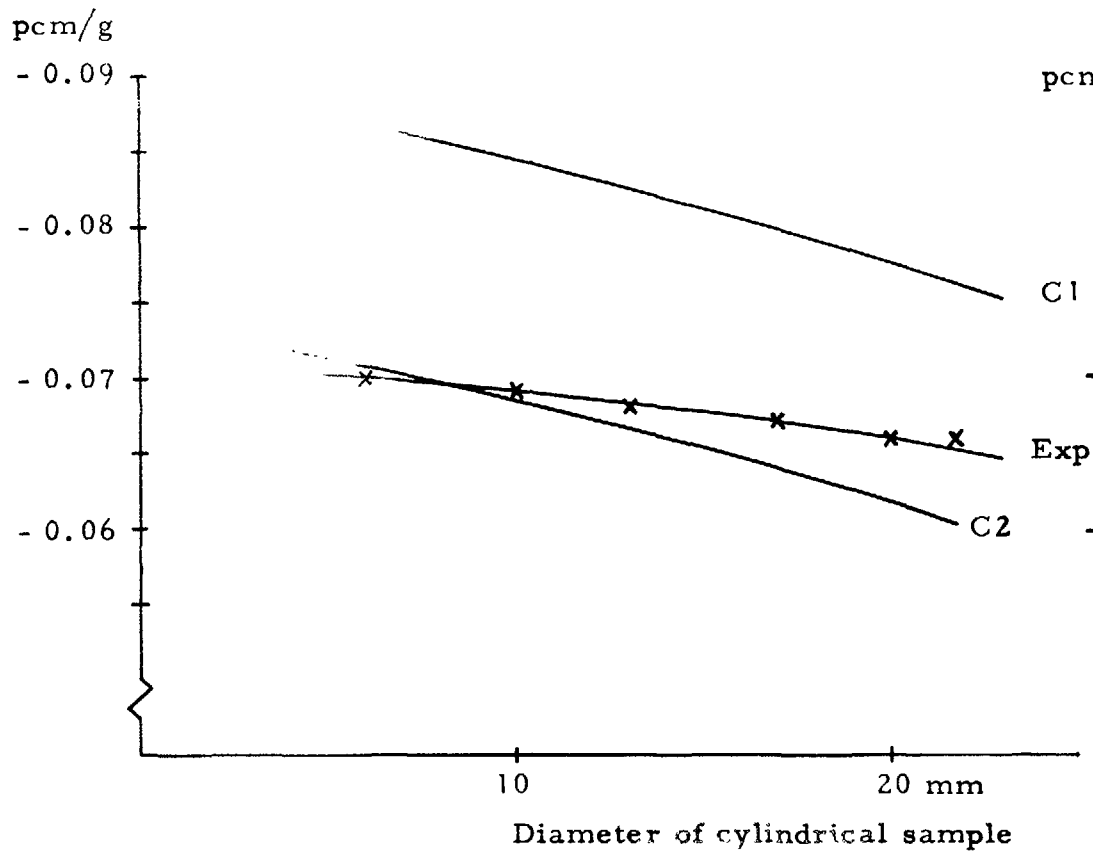
Fig. 11 a

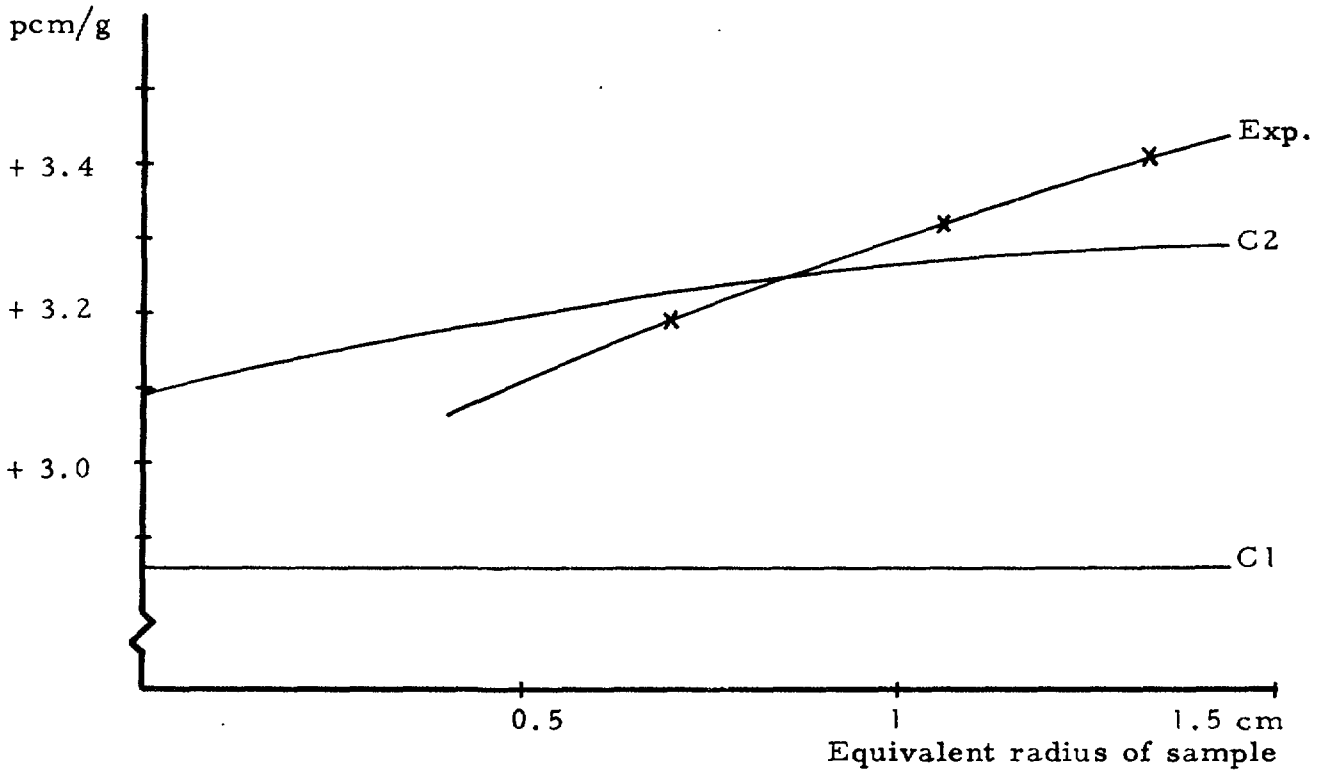Sample size dependence of reactivity coefficient
of copper in Assembly 3
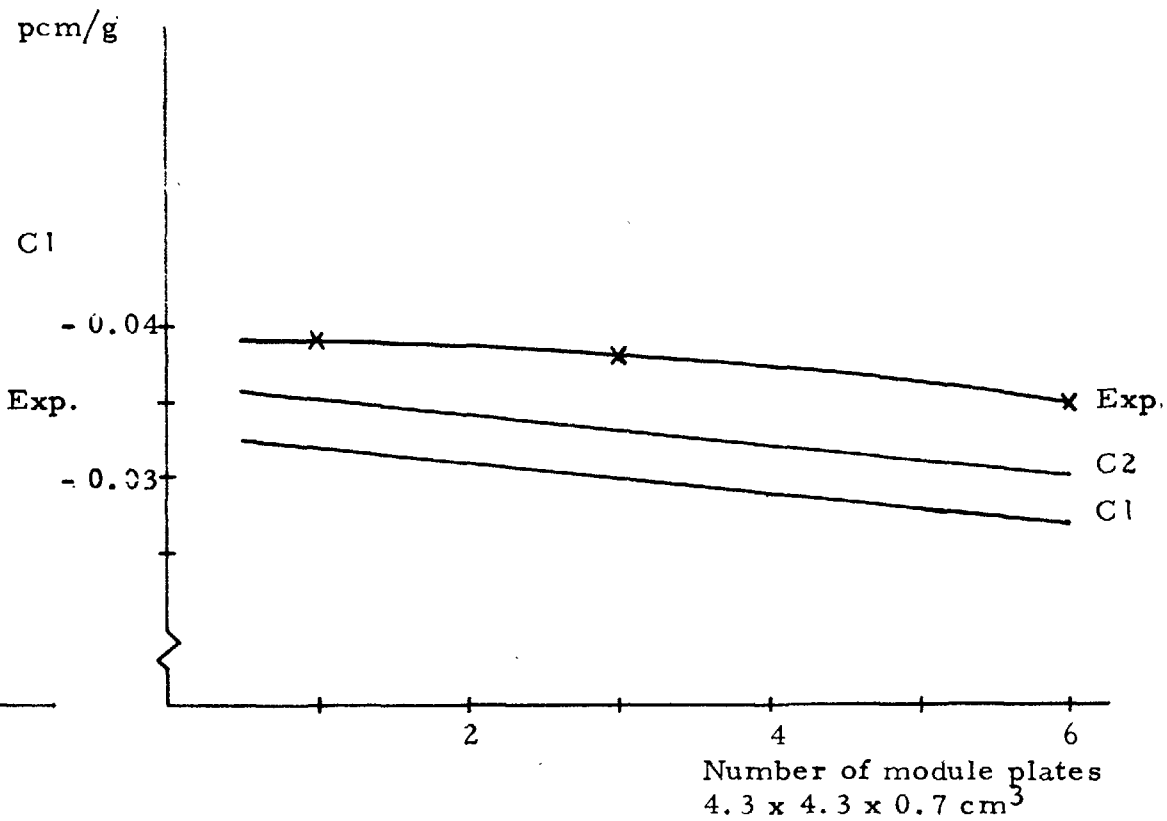
Fig. 11 b

Sample size dependence of reactivity coefficient
of iron in Assembly 3
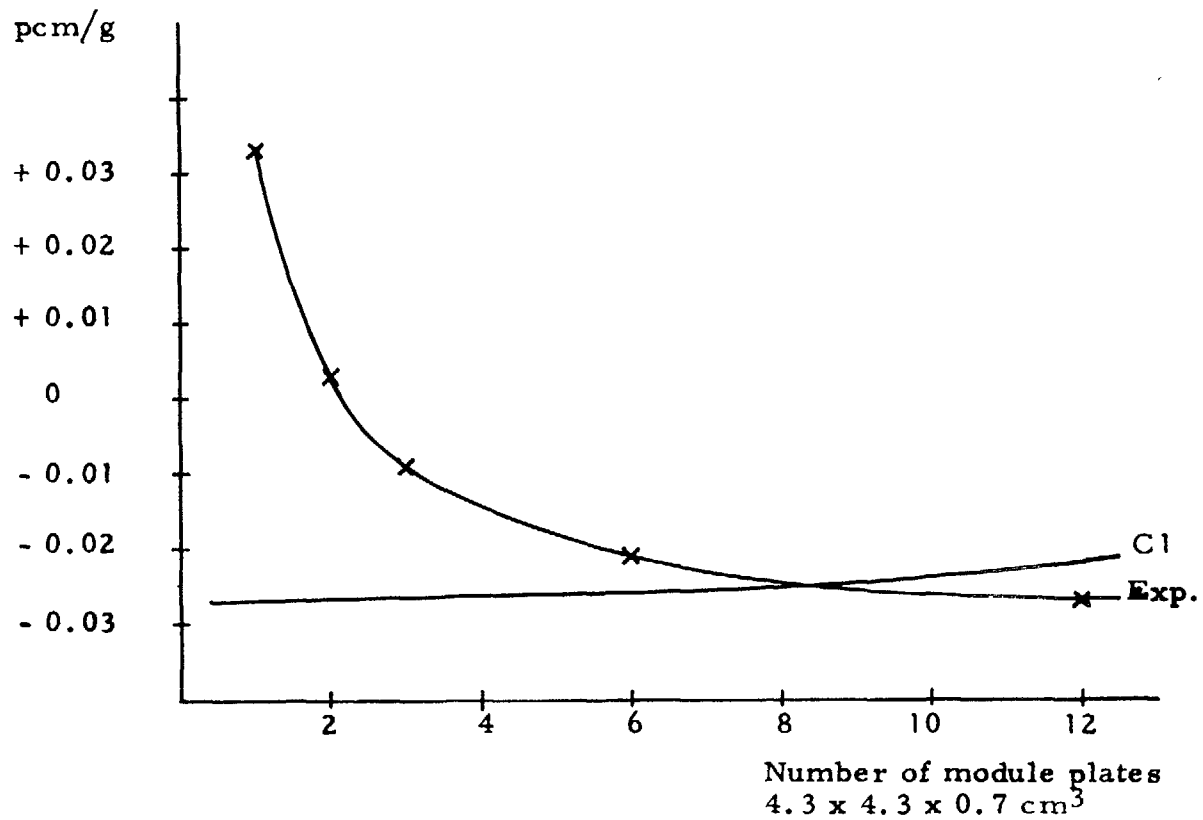
Fig. 12 a

Sample size dependence of reactivity coefficient
of aluminium in Assembly 1
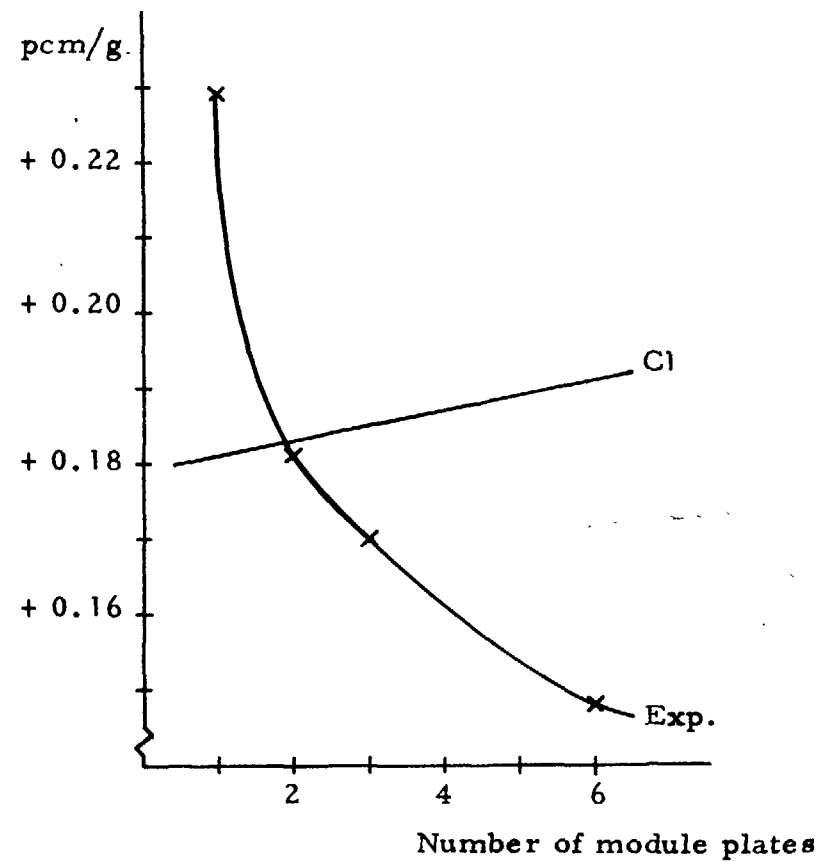
Fig. 12 b

Sample size dependence of reactivity
coefficient of carbon in Assembly 1

Fig. 13 b

Sample size dependence of reactivity coefficient of diphenyl in Assembly 3

Fig. 13 a

Sample size dependence of reactivity coefficient of diphenyl in Assembly 1
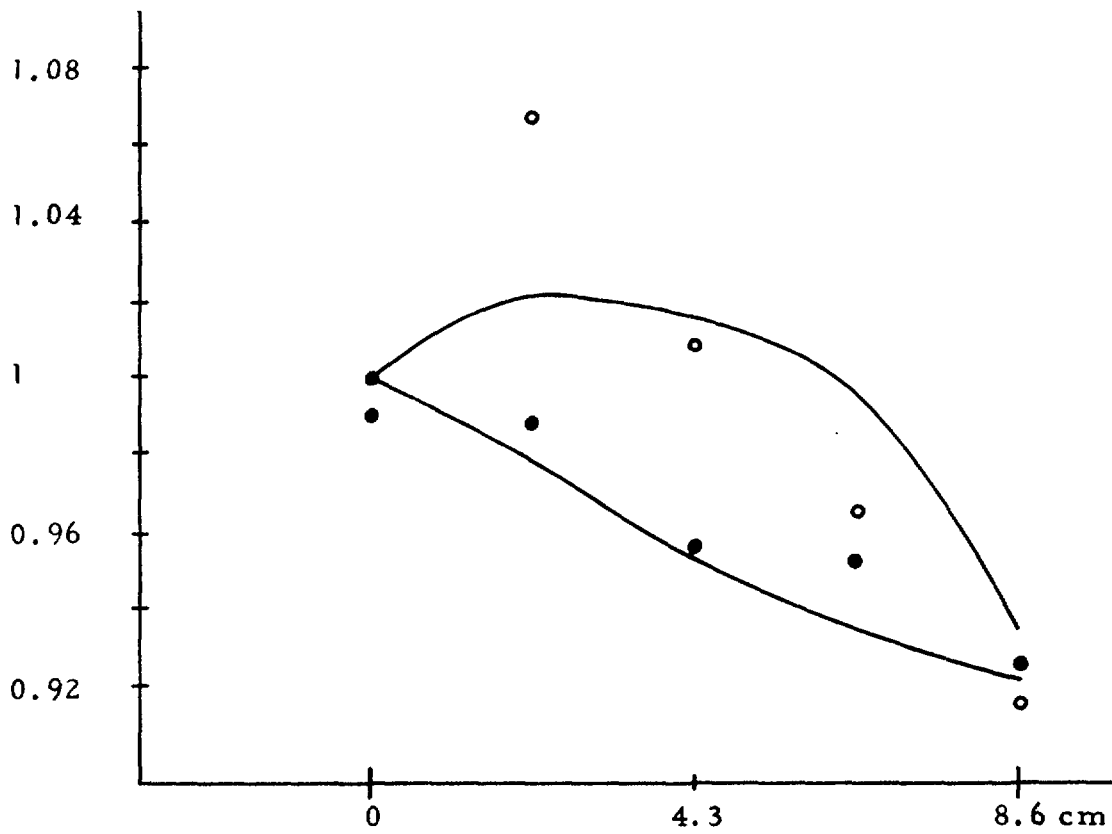
Fig. 14 a

In115(n, n') reaction rates in a chamber containing carbon between
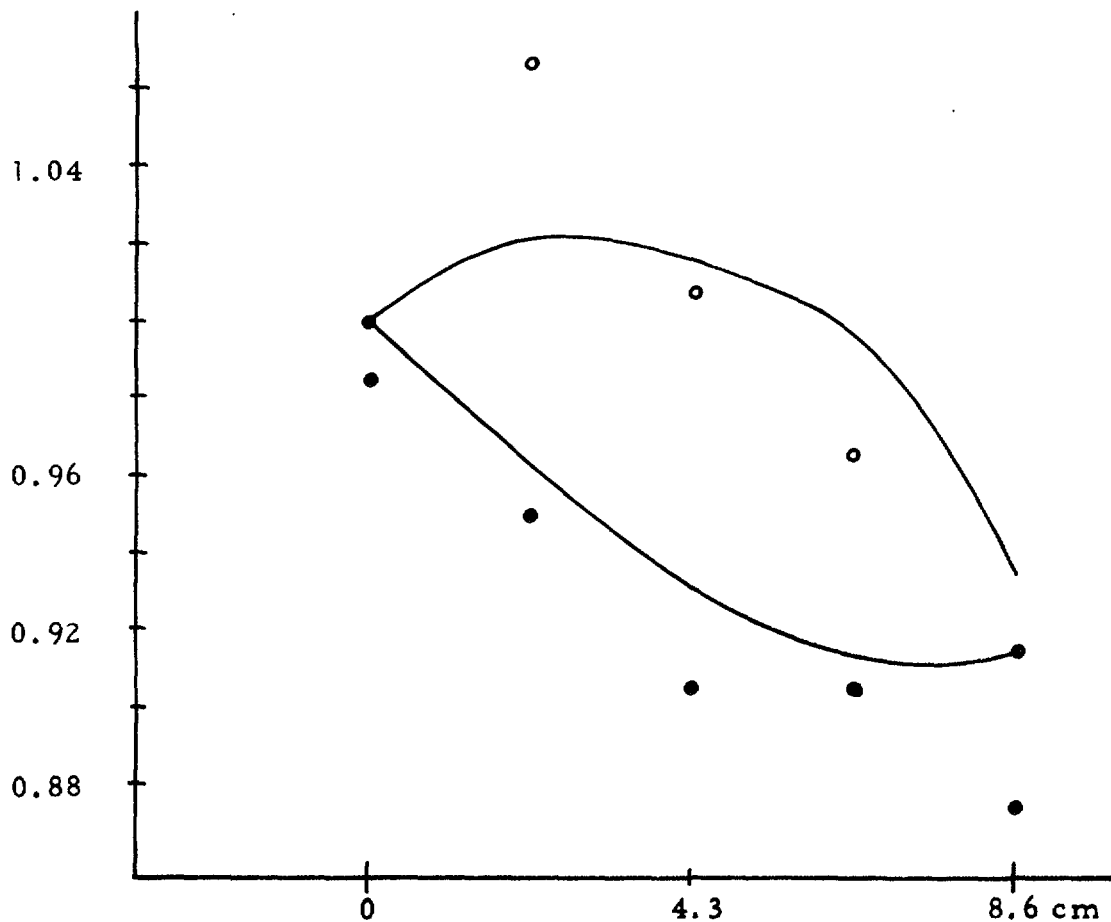2.15 and 6.45 cm and in an empty chamber

Fig. 14 b

In115(n, n') reaction rates in a chamber containing iron between
2.15 and 6.45 cm and in an empty chamber

Distances from lower end of chambers. Filled points: Chamber with sample.
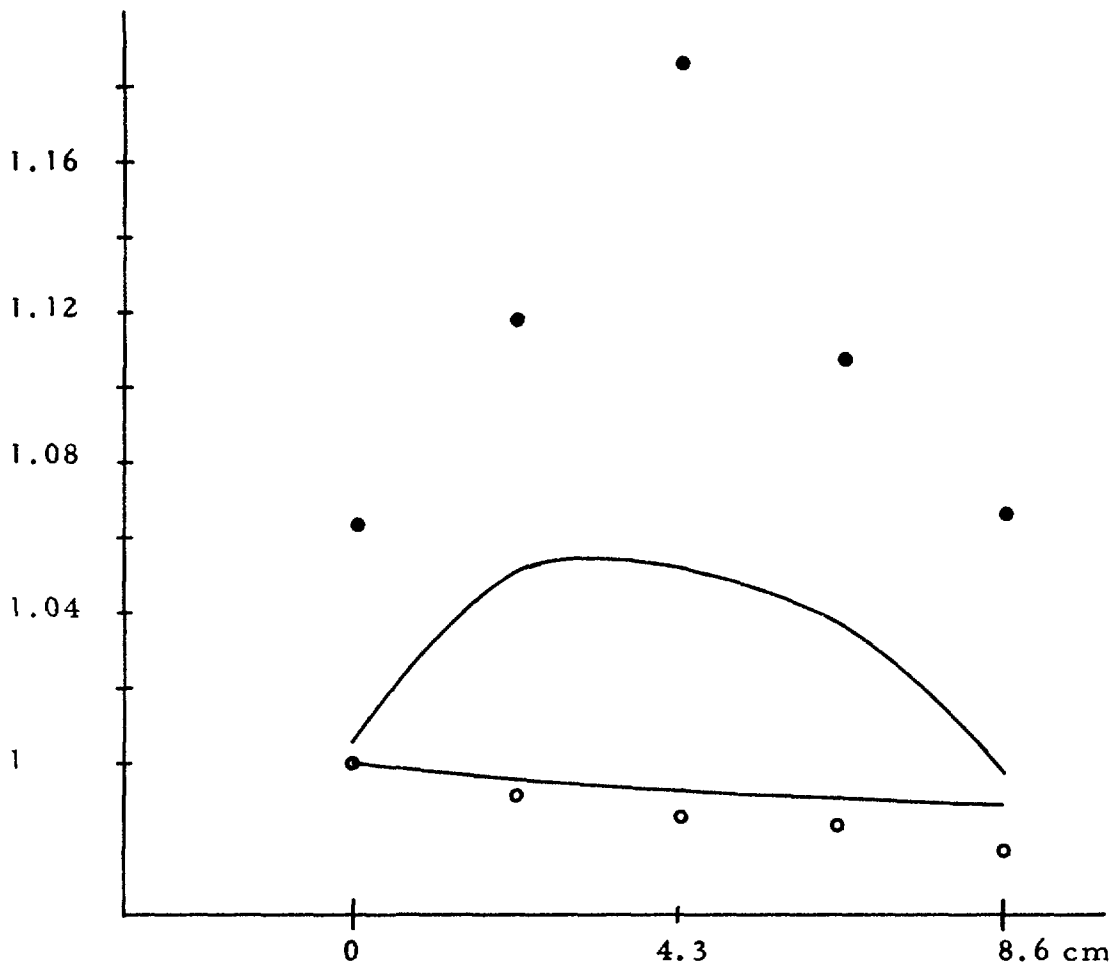Full lines: Calculated values.   Rings: Empty chamber.

Fig. 15 a

Au197(n,γ) reaction rates in a chamber containing carbon between
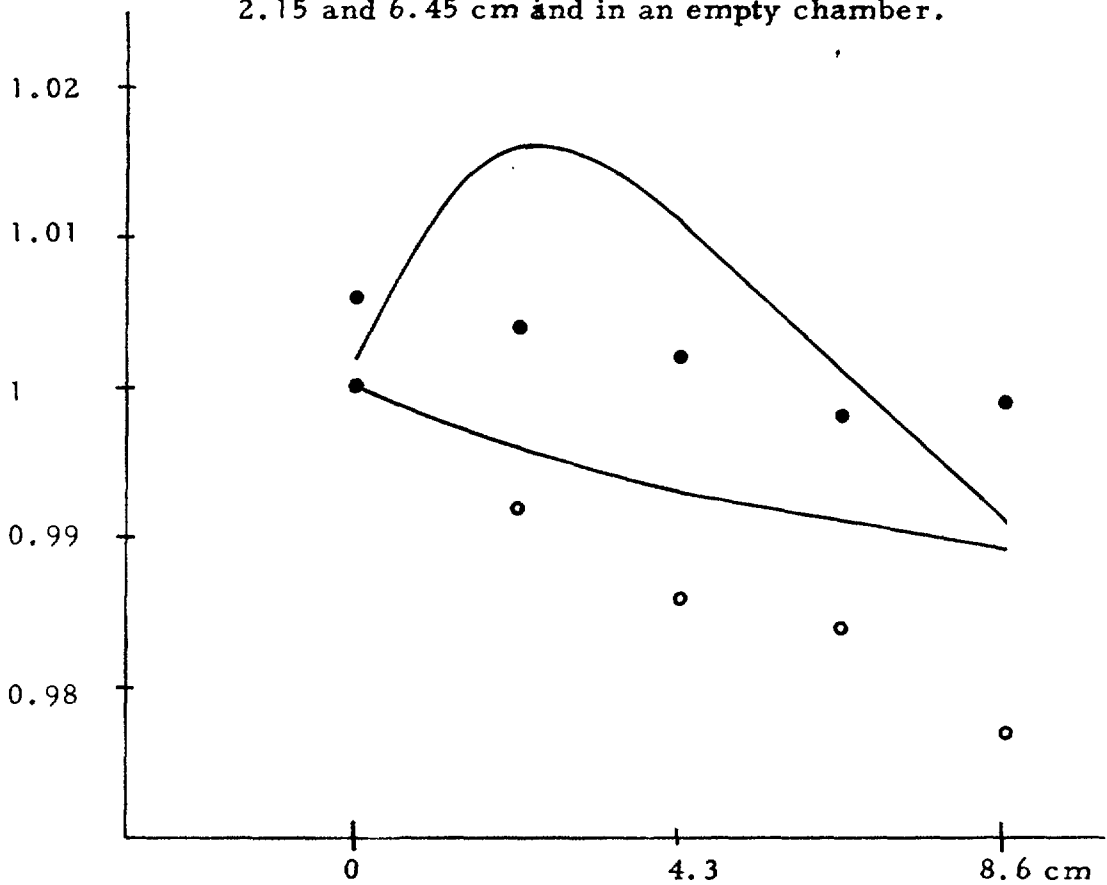2.15 and 6.45 cm and in an empty chamber.

Fig. 15 b

Au197(n,γ) reaction rates in a chamber containing iron between
2.15 and 6.45 cm and in an empty chamber.

Distances from lower end of chambers. Filled points: Chamber with sample.
Rings: Empty chamber.   Full lines: Calculated curves.

LIST OF PUBLISHED AE-REPORTS

1—135. (See the back cover earlier reports.)

136. Ejection of uranium atoms from UO_2 by fission fragments. By G. Nilsson. 1964. 38 p. Sw. cr. 8:—.

137. Personell neutron monitoring at AB Atomenergi. By S. Hagsgård and C.-O. Widell. 1964. 11 p. Sw. cr. 8:—.

138. Radiation induced precipitation in iron. By B. Solly. 1964. 8 p. Sw. cr. 8:—.

139. Angular distributions of neutrons from (p, n)-reactions in some mirror nuclei. By L. G. Strömberg, T. Wiedling and B. Holmqvist. 1964. 28 p. Sw. cr. 8:—.

140. An extended Greuling-Goertzel approximation with a P_n -approximation in the angular dependence. By R. Håkansson. 1964. 21 p. Sw. cr. 8:—.

141. Heat transfer and pressure drop with rough surfaces, a literature survey. By A. Bhattachayya. 1964. 78 p. Sw. cr. 8:—.

142. Radiolysis of aqueous benzene solutions. By H. Christensen. 1964. 50 p. Sw. cr. 8:—.

143. Cross section measurements for some elements suited as thermal spectrum indicators: Cd, Sm, Gd and Lu. By E. Sokolowski, H. Pekarek and E. Jonsson. 1964. 27 p. Sw. cr. 8:—.

144. A direction sensitive fast neutron monitor. By B. Antolkovic, B. Holmqvist and T. Wiedling. 1964. 14 p. Sw. cr. 8:—.

145. A user's manual for the NRN shield design method. By L. Hjärne. 1964. 107 p. Sw. cr. 10:—.

146. Concentration of 24 trace elements in human heart tissue determined by neutron activation analysis. By P. O. Wester. 1964. 33 p. Sw. cr. 8:—.

147. Report on the personnel Dosimetry at AB Atomenergi during 1963. By K.-A. Edvardsson and S. Hagsgård. 1964. 16 p. Sw. cr. 8:—.

148. A calculation of the angular moments of the kernel for a manatomic gas scatterer. By R. Håkansson. 1964. 16 p. Sw. cr. 8:—.

149. An anion-exchange method for the separation of P-32 activity in neutron-irradited biological material. By K. Samsahl. 1964. 10 p. Sw. cr 8:—.

150. Inelastic neutron scattering cross sections of Cu^{63} and Cu^{65} in the energy region 0.7 to 1.4 MeV. By B. Holmqvist and T. Wiedling. 1964. 30 p. Sw. cr. 8:—.

151. Determination of magnesium in needle biopsy samples of muscle tissue by means of neutron activation analysis. By D. Brune and H. E. Sjöberg. 1964. 8 p. Sw. cr. 8:—.

152. Absolute El transition probabilities in the doformed nuclei Yb^{177} and Hf^{179}. By Sven G. Malmskog. 1964. 21 p. Sw. cr. 8:—.

153. Measurements of burnout conditions for flow of boiling water in vertical 3-rod and 7-rod clusters. By K. M. Becker, G. Hernborg and J. E. Flinta. 1964. 54 p. Sw. cr. 8:—.

154. Integral parameters of the thermal neutron scattering law. By S. N. Purohit. 1964. 48 p. Sw. cr. 8:—.

155. Tests of neutron spectrum calculations with the help of foil measurments in a D_2O and in an H_2O-moderated reactor and in reactor shields of concrete and iron. By R. Nilsson and E. Aalto. 1964. 23 p. Sw. cr. 8:—.

156. Hydrodynamic instability and dynamic burnout in natural circulation two-phase flow. An experimental and theoretical study. By K. M. Becker. S. Jahnberg, I. Haga, P. T. Hansson and R. P. Mathisen. 1964. 41 p. Sw. cr. 8:—.

157. Measurements of neutron and gamma attenuation in massive laminated shields of concrete and a study of the accuracy of some methods of calculation. By E. Aalto and R. Nilsson. 1964. 110 p. Sw. cr. 10:—.

158. A study of the angular distributions of neutrons from the Be^9 (p,n) B^9 reaction at low proton energies. By. B. Antolkovic', B. Holmqvist and T. Wiedling. 1964. 19 p. Sw. cr. 8:—.

159. A simple apparatus for fast ion exchange separations. By K. Samsahl. 1964. 15 p. Sw. cr. 8:—.

160. Measurements of the Fe^{54} (n, p) Mn^{54} reaction cross section in the neutron energy range 2.3—3.8 MeV. By A. Lauber and S. Malmskog. 1964. 13 p. Sw. cr. 8:—.

161. Comparisons of measured and calculated neutron fluxes in laminated iron and heavy water. By. E. Aalto. 1964. 15. p. Sw. cr. 8:—.

162. A needle-type p-i-n junction semiconductor detector for in-vivo measurement of beta tracer activity. By A. Lauber and B. Rosencrantz. 1964. 12 p. Sw. cr. 8:—.

163. Flame spectro photometric determination of strontium in water and biological material. By G. Jönsson. 1964. 12 p. Sw. cr. 8:—.

164. The solution of a velocity-dependent slowing-down problem using case's eigenfunction expansion. By A. Claesson. 1964. 16 p. Sw. cr. 8:—.

165. Measurements of the effects of spacers on the burnout conditions for flow of boiling water in a vertical annulus and a vertical 7-rod cluster. By K. M. Becker and G. Hernberg. 1964. 15 p. Sw. cr. 8:—.

166. The transmission of thermal and fast neutrons in air filled annular ducts through slabs of iron and heavy water. By J. Nilsson and R. Sandlin. 1964. 33 p. Sw. cr. 8:—.

167. The radio-thermoluminescense of $CaSO_4$: Sm and its use in dosimetry. By B. Bjärngard. 1964. 31 p. Sw. cr. 8:—.

168. A fast radiochemical method for the determination of some essential trace elements in biology and medicine. By K. Samsahl. 1964. 12 p. Sw. cr. 8:—.

169. Concentration of 17 elements in subcellular fractions of beef heart tissue determined by neutron activation analysis. By P. O. Wester. 1964. 29 p. Sw. cr. 8:—.

170. Formation of nitrogen-13, fluorine-17, and fluorine-18 in reactor-irradiated H_2O and D_2O and applications to activation analysis and fast neutron flux monitoring. By L. Hammar and S. Forsén. 1964. 25 p. Sw. cr. 8:—.

171. Measurements on background and fall-out radioactivity in samples from the Baltic bay of Tvären, 1957—1963. By P. O. Agnedal. 1965. 48 p. Sw. cr. 8:—.

172. Recoil reactions in neutron-activation analysis. By D. Brune. 1965. 24 p. Sw. cr. 8:—.

173. A parametric study of a constant-Mach-number MHD generator with nuclear ionization. By J. Braun. 1965. 23 p. Sw. cr. 8:—.

174. Improvements in applied gamma-ray spectrometry with germanium semiconductor dector. By D. Brune, J. Dubois and S. Hellström. 1965. 17 p. Sw. cr. 8:—.

175. Analysis of linear MHD power generators. By E. A. Witalis. 1965. 37 p. Sw. cr. 8:—.

176. Effect of buoyancy on forced convection heat transfer in vertical channels — a literature survey. By A. Bhattacharyya. 1965. 27 p. Sw. cr. 8:—.

177. Burnout data for flow of boiling water in vertical round ducts, annuli and rod clusters. By K. M. Becker, G. Hernborg, M. Bode and O. Eriksson. 1965. 109 p. Sw. cr. 8:—.

178. An analytical and experimental study of burnout conditions in vertical round ducts. By K. M. Becker. 1965. 161 p. Sw. cr. 8:—.

179. Hindered El transitions in Eu^{155} and Tb^{161}. By S. G. Malmskog. 1965. 19 p. Sw. cr. 8:—.

180. Photomultiplier tubes for low level Cerenkov detectors. By O. Strindehag. 1965. 25 p. Sw. cr. 8:—.

181. Studies of the fission integrals of U235 and Pu239 with cadmium and boron filters. By E. Hellstrand. 1965. 32 p. Sw. cr. 8:—.

182. The handling of liquid waste at the research station of Studsvik, Sweden. By S. Lindhe and P. Linder. 1965. 18 p. Sw. cr. 8:—.

183. Mechanical and instrumental experiences from the erection, commissioning and operation of a small pilot plant for development work on aqueous reprocessing of nuclear fuels. By K. Jönsson. 1965. 21 p. Sw. cr. 8:—.

184. Energy dependent removal cross-sections in fast neutron shielding theory. By H. Grönroos. 1965. 75 p. Sw. cr. 8:—.

185. A new method for predicting the penetration and slowing-down of neutrons in reactor shields. By L. Hjärne and M. Leimdörfer. 1965. 21 p. Sw. cr. 8:—.

186. An electron microscope study of the thermal neutron induced loss in high temperature tensile ductility of Nb stabilized austenitic steels. By R. B. Roy. 1965. 15 p. Sw. cr. 8:—.

187. The non-destructive determination of burn-up means of the Pr-144 2.18 MeV gamma activity. By R. S. Forsyth and W. H. Blackadder. 1965. 22 p. Sw. cr. 8:—.

188. Trace elements in human myocardial infarction determined by neutron activation analysis. By P. O. Wester. 1965. 34 p. Sw. cr. 8:—.

189. An electromagnet for precession of the polarization of fast-neutrons. By O. Aspelund, J. Björkman and G. Trumpy. 1965. 28 p. Sw. cr. 8:—.

190. On the use of importance sampling in particle transport problems. By B. Eriksson. 1965. 27 p. Sw. cr. 8:—.

191. Trace elements in the conductive tissue of beef heart determined by neutron activation analysis. By P. O. Wester. 1965. 19 p. Sw. cr. 8:—.

192. Radiolysis of aqueous benzene solutions in the presence of inorganic oxides. By H. Christensen. 12 p. 1965. Sw. cr. 8:—.

193. Radiolysis of aqueous benzene solutions at higher temperatures. By H. Christensen. 1965. 14 p. Sw. cr. 8:—.

194. Theoretical work for the fast zero-power reactor FR-0. By H. Häggblom. 1965. 46 p. Sw. cr. 8:—.

195. Experimental studies on assemblies 1 and 2 of the fast reactor FR0. Part 1. By T. L. Andersson, E. Hellstrand, S-O. Londen and L. I. Tirén. 1965. 45 p. Sw. cr. 8:—.

196. Measured and predicted variations in fast neutron spectrum when penetrating laminated Fe-D_2O. By E. Aalto, R. Sandlin and R. Fräki. 1965. 20 p. Sw. cr. 8:—.

197. Measured and predicted variations in fast neutron spectrum in massive shields of water and concrete. By E. Aalto, R. Fräki and R. Sandlin. 1965. 27 p. Sw. cr. 8:—.

198. Measured and predicted neutron fluxes in, and leakage through, a configuration of perforated Fe plates in D_2O. By E. Aalto. 1965. 23 p. Sw. cr. 8:—.

199. Mixed convection heat transfer on the outside of a vertical cylinder. By A. Bhattacharyya. 1965. 42 p. Sw. cr. 8:—.

200. An experimental study of natural circulation in a loop with parallel flow test sections. By R. P. Mathisen and O. Eklind. 1965. 47 p. Sw. cr. 8:—.

201. Heat transfer analogies. By A. Bhattachoryya. 1965. 55 p. Sw. cr. 8:—.

202. A study of the "384" KeV complex gamma emission from plutonium-239. By R. S. Forsyth and N. Ronqvist. 1965. 14 p. Sw. cr. 8:—.

203. A scintillometer assembly for geological survey. By E. Dissing and O. Landström. 1965. 16 p. Sw. cr. 8:—.

204. Neutron-activation analysis of natural water applied to hydrogeology. By O. Landström and C. G. Wenner. 1965. 28 p. Sw. cr. 8:—.

205. Systematics of absolute gamma ray transition probabilities in deformed odd-A nuclei. By S. G. Malmskog. 1965. 60 p. Sw. cr. 8:—.

206. Radiation induced removal of stacking faults in quenched aluminium. By U. Bergenlid. 1965. 11 p. Sw. cr. 8:—.

207. Experimental studies on assemblies 1 and 2 of the fast reactor FR0. Part 2. By E. Hellstrand, T. L. Andersson, B. Brunfelter, J. Kockum, S-O. Londen and L. I. Tirén. 1965. 50 p. Sw. cr. 8:—.

208. Measurement of the neutron slowing-down time distribution at 1.46 eV and its space dependence in water. By E. Möller. 1965. 29. p. Sw. cr. 8:—.

209. Incompressible steady flow with tensor conductivity leaving a transverse magnetic field. By E. A. Witalis. 1965. 17 p. Sw. cr. 8:—.

210. Methods for the determination of currents and fields in steady two-dimensional MHD flow with tensor conductivity. By E. A. Witalis. 1965. 13 p. Sw. cr. 8:—.

211. Report on the personnel dosimetry at AB Atomenergi during 1964. By K. A. Edvardsson. 1966. 15 p. Sw. cr. 8:—.

212. Central reactivity measurements on assemblies 1 and 3 of the fast reactor FR0. By S-O. Londen. 1966. 58 p. Sw. cr. 8:—.

Förteckning över publicerade AES-rapporter

1. Analys medelst gamma-spektrometri. Av D. Brune. 1961. 10 s. Kr 6:—.

2. Bestrålningsförändringar och neutronatmosfär i reaktortrycktankar — några synpunkter. Av M. Grounes. 1962. 33 s. Kr 6:—.

3. Studium av sträckgränsen i mjukt stål. Av G. Ostberg och R. Attermo. 1963. 17 s. Kr 6:—.

4. Teknisk upphandling inom reaktorområdet. Av Erik Jonson. 1963. 64 s. Kr 8:—.

5. Agesta Kraftvärmeverk. Sammanställning av tekniska data, beskrivningar m. m. för reaktordelen. Av B. Lilliehöök. 1964. 336 s. Kr 15:—.